Revisiting the involvement of tau in complex neural network remodeling: analysis of the extracellular neuronal activity in organotypic brain slice co-cultures

Thomas Bouillet, Manuel Ciba, Caroline Lourenço Alves, Francisco Aparecido Rodrigues, Christiane Thielemann, Morvane Colin, Luc Buée, Sophie Halliez

Title: Revisiting the involvement of tau in complex neural network remodeling: analysis of the extracellular neuronal activity in organotypic brain slice co-cultures

Authors: Thomas Bouillet[1]*, Manuel Ciba[2]*, Caroline Lourenço Alves[2,3], Francisco Aparecido Rodrigues[3], Christiane Thielemann[2], Morvane Colin[1], Luc Buée[1], Sophie Halliez[1]

Authors' affiliations:

[1]Univ. Lille, Inserm, CHU Lille, U1172 - LilNCog - Lille Neuroscience & Cognition, F-59000 Lille, France

[2]Biomems lab, University of Applied Sciences Aschaffenburg, 63743 Aschaffenburg, Germany

[3]Institute of Mathematics and Computer Science, University of São Paulo - São Carlos, SP 13566-590, Brazil

*Same contribution

Corresponding author(s): Manuel.Ciba@th-ab.de & sophie.halliez@univ-lille.fr

Conflict of interest statement: The authors have no competing financial interests to declare.

Keywords: Tau, Neural networks, Hippocampus, Entorhinal cortex, Neuronal activity, Synchrony, Connectivity, Excitation/inhibition ratio

ABSTRACT

Objective: Tau ablation has a protective effect in epilepsy due to inhibition of the hyperexcitability/hypersynchrony. Protection may also occur in transgenic models of Alzheimer's disease by reducing the epileptic activity and normalizing the excitation/inhibition imbalance. However, it is difficult to determine the exact functions of tau, because tau knockout (tau^{KO}) brain

networks exhibit elusive phenotypes. In this study, we aimed to further explore the physiological role of tau using brain network remodeling.

Approach: The effect of tau ablation was investigated in hippocampal-entorhinal slice co-cultures during network remodeling. We recorded the spontaneous extracellular neuronal activity over two weeks in single-slice cultures and co-cultures from control and *tau*^{KO} mice. We compared the burst parameters and applied concepts and analytical tools intended for the analysis of the network synchrony and connectivity.

Main results: Comparison of the control and *tau*^{KO} co-cultures revealed that tau ablation had an anti-synchrony effect on the hippocampal-entorhinal two-slice networks at late stages of culture, in line with the literature. Differences were also found between the single-slice and co-culture conditions, which indicated that tau ablation had differential effects at the sub-network scale. For instance, tau ablation was found to have an anti-synchrony effect on the co-cultured hippocampal slices throughout the culture, possibly due to a reduction in the excitation/inhibition ratio. Conversely, tau ablation led to increased synchrony in the entorhinal slices at early stages of the co-culture, possibly due to homogenization of the connectivity distribution.

Significance: The new methodology presented here proved useful for investigating the role of tau in the remodeling of complex brain-derived neural networks. The results confirm previous findings and hypotheses concerning the effects of tau ablation on neural networks. Moreover, the results suggest, for the first time, that tau has multifaceted roles that vary in different brain sub-networks.

INTRODUCTION

Tau is a microtubule-associated protein encoded by the *MAPT (Microtubule-Associated Protein Tau*) gene. It is known to be involved in Alzheimer's disease (AD) and other tauopathies, which together form a heterogeneous group of neurodegenerative disorders. These diseases are characterized by the abnormal intracellular aggregation of tau, which culminates in the formation of neurofibrillary tangles

47 in AD. Dysfunction of the brain networks occurs, as well as a loss of neurons and synapses, which
48 ultimately results in cognitive deficits. There is also evidence that there is an imbalance in neuronal
49 excitation/inhibition (E/I) in the early stages of AD, which may be central in the disease evolution
50 (Maestú et al., 2021).

51 It is currently thought that the progression of AD involves the transneuronal transportation of
52 pathological tau from primary sites to anatomically connected regions, which then leads to further tau
53 aggregation (Colin et al., 2020). The observation of a pattern of disease progression has led to the
54 staging of AD pathology (Braak and Braak, 1991; Braak and Del Tredici, 2016). However, recent work
55 on machine learning has indicated that there may be four different spatiotemporal patterns of tau
56 deposition, as opposed to a single canonical one (Vogel et al., 2021). Nevertheless, it is clear that
57 certain brain regions are first affected by the pathology, including the entorhinal cortex and the
58 hippocampus. These two regions are interconnected and they are known to play a major role in
59 memory and spatial navigation (Ohara et al., 2018; Witter et al., 2017). According to a model of
60 pathological tau spreading, the entorhinal cortex may be the 'epicenter region' from which the
61 pathology spreads (Vogel et al., 2020). This structure is known to be the main gateway for
62 communication between the neocortex and the hippocampal formation. Its superficial layers convey
63 much of the sensory information that is processed by the hippocampal formation, while its deep layers
64 relay processed information back to the neocortex.

65 The functions of tau have been extensively studied, mainly because of its involvement in AD, but also
66 because tau reduction in mice has been found to protect against epilepsy (DeVos et al., 2013; Holth et
67 al., 2013; Putra et al., 2020). The functions have been found to be multifaceted (Kent et al., 2020;
68 Sotiropoulos et al., 2017), with evidence that it is involved in neuronal differentiation (Sapir et al.,
69 2012; Sennvik et al., 2007), neurite outgrowth and maturation (Fuster-Matanzo et al., 2012; Paglini et
70 al., 2000), axonal transport (Lacovich et al., 2017), axon initial segment organization (Chang et al.,
71 2021), and synaptic architecture (Ittner et al., 2010). Electrophysiology experiments on acute brain

slices from tau knockout mice (*Mapt*$^{-/-}$ or *tau*^{KO}) have shown that basal synaptic transmission is unaltered by the absence of tau (Ahmed et al., 2014; Biundo et al., 2018), but that there is a reduction in the spontaneous firing and E/I ratio of excitatory pyramidal cells, as well as an increase in the excitability of inhibitory interneurons (Chang et al., 2021). Long-term potentiation/depression has also been found to be altered in *tau*^{KO} adult mice, thus indicating that tau plays a role in synaptic plasticity (Ahmed et al., 2014; Biundo et al., 2018; Kimura et al., 2014). At the network scale, it is thought that tau ablation leads to a reduction in the E/I imbalance and hence to a reduction in neural network hypersynchrony and/or hyperexcitability (Chang et al., 2021; Roberson et al., 2011). This could explain why tau reduction has protective effects in epilepsy and possibly also in AD models. Altogether, this work indicates the complexity of tau's involvement in neural networks, which is still being explored.

Organotypic brain slice cultures are a promising tool for investigating the processes that underlie brain disorders. The slice cultures are intrinsically pre-existing three-dimensional brain networks. Neural networks within single-slice cultures undergo a certain amount of *in vitro* remodeling. However, when two brain slices are co-cultured, a two-slice network can be formed, which involves a larger amount of remodeling. In this study, our idea was to use brain-slice co-cultures to reveal subtle alterations caused by tau ablation. For this, we recorded the spontaneous extracellular neuronal activity over two weeks in single-slice cultures and hippocampal-entorhinal co-cultures prepared from *wild-type* (*WT*) and *tau*^{KO} mice. The burst parameters were examined in order to identify differences between networks established from different brain regions (hippocampus and entorhinal cortex) as well as alterations resulting from tau ablation. Concepts and analytical tools intended for the study of network synchrony and connectivity were used to determine how tau ablation affects the hippocampal and entorhinal networks in single-slice and co-culture conditions. In this way, we aimed to decipher the role of tau in neural network remodeling.

METHOD

Organotypic brain slice cultures on micro-electrode arrays (MEAs)

The experiments were carried out with the approval of an ethics committee (agreement APAFIS#2264-2015101320441671 from CEEA75, Lille, France) and followed the European guidelines for the use of animals in research.

C57BL/6JRj pregnant mice (Janvier Labs) and *Mapt*$^{+/-}$ mice (Tucker et al., 2001) were housed in a temperature-controlled (20–22° C) room with a 12-hour light, 12-hour dark cycle. Food and water were provided *ad libitum*. For the first set of experiments, the brains were dissected from 7-day-old C57BL/6JRj mice; for the second set of experiments, the brains were from 5-day-old mice obtained from breeding the *Mapt*$^{+/-}$ mice. The dissection was performed in ice-cold Gey's balanced salt solution (GBSS, Sigma), which was supplemented with the glutamate receptor antagonist kynurenic acid (1 mM; Sigma) and glucose (33 mM; Sigma). The *Mapt*$^{+/+}$, *Mapt*$^{+/-}$, and *Mapt*$^{-/-}$ brains were identified using a fluorescence microscope (Leica DM IL LED), as the *Mapt* knock-out results from the insertion of the green fluorescent protein (GFP) sequence into *Mapt.* Although both the *Mapt*$^{+/-}$ and *Mapt*$^{-/-}$ (or *tau*^{KO}) brains were positive for GFP, the intensity was greater for the latter. The *Mapt* genotype was later confirmed using polymerase chain reaction (PCR) on DNA extracted from the pups' tails.

A vibratome (VT1200S, Leica) was used to cut 350-µm-thick slices in the GBSS-based solution. The hippocampus and entorhinal cortex were then micro-dissected, and these slices were transferred onto MEAs (60MEA200/30iR-Ti with glass rings, Multi Channel Systems) encompassing 59 recording electrodes and one reference electrode. The slices were cultured in sterile slice culture medium (SCM; 150 µl), which was composed of 50% Eagle's minimum essential medium (Lonza), 25% Basal Medium Eagle (Lonza), and 25% heat-inactivated horse serum (Gibco); the medium was supplemented with glucose, Antibiotic-Antimycotic (Gibco), and L-glutamine (Gibco). Before being used, the MEAs were cleaned by immersion in ethanol, and then air-dried in a sterile class II biosafety cabinet (Thermo Scientific PSM HERASAFE KS) for 48 hours. The MEA recording area was coated with a mixture of Poly-D-lysine (0.5 mg/ml, Sigma) and laminin (10 µg/ml, Sigma). The coating solution was applied for 30 minutes at room temperature, and then washed using sterile water (Corning) and air-dried. The slices

were plated onto the MEAs using a microscope. For the first set of co-cultures (from the C57BL/6JRj mice), the entorhinal and hippocampal slices were placed either contiguously or at least 4 mm apart, in order to enable or prevent the formation of inter-slice connections, respectively. For the second set of co-cultures (from the *Mapt*$^{+/+}$ and *Mapt*$^{-/-}$ mice), the entorhinal and hippocampal slices were placed approximately 150 µm apart in order to facilitate the electrode labelling (as either entorhinal or hippocampal). After 10 minutes, the medium was replaced by fresh medium and the MEA culture chamber was sealed using a removable, hydrophobic, semipermeable membrane cover (fluorinated ethylene-propylene, 12.5 microns thick, Multi Channel Systems). The slices were cultured at 37°C in a humidified atmosphere containing 5% CO_2 and the culture medium was changed once a day. At the end of the slice culture period, the MEAs were first washed in water and then in 1% Tergazyme (Alconox) for two hours at room temperature. The MEAs were then stored in water at 4°C.

Extracellular recordings of neuronal activity

Extracellular recordings were obtained using the MEA2100-System (Multi Channel Systems), which included a Headstage for 2 x 60 channels (Multi Channel Systems; for signal amplification and digitization), an interface board (MCS-IFB, Multi Channel Systems), and a personal computer. A temperature controller (TC02, Multi Channel Systems) was used to maintain the culture temperature at 37°C during the recording sessions. Real-time monitoring, signal filtering, and spike detection were carried out using the Multi Channel Experimenter software (Multi Channel Systems). The recordings were obtained after 4, 6, 8, 10, and 12 days *in vitro* (DIV) for the first set of experiments, and after 3, 4, 6, 8, 10, 12, and 14 DIV for the second set of experiments. Before each recording session, 150 µl of SCM was added to the cultures. This was followed by a period of 15 minutes' rest into the experimental setup and then the neuronal activity was recorded for a total of 5 minutes. Spikes were detected on the basis of an amplitude threshold, which was set for each recording electrode. This value was calculated as the standard deviation of the baseline noise level, multiplied by -10.

Analysis of the burst parameters

Spike timestamps were recorded using the Multi Channel Experimenter software and exported in NEX format using the Multi Channel DataManager software (Multi Channel Systems). Burst analysis was carried out using Neuroexplorer software (Nex Technologies). For the slice co-cultures, each electrode was labelled as either entorhinal or hippocampal based on pictures taken after plating. If there was any ambiguity, the electrode was excluded from the analysis. Electrodes that had at least 25 spikes during the 5-minute recordings were defined as active electrodes. The burst analysis was based on an interval algorithm that used the following parameters: maximal interval to start burst: 0.01 s; minimal interval between bursts: 0.01 s; minimum interval between bursts: 0.01 s; minimum burst duration: 0.02 s; and a minimum of four spikes in a burst. For each electrode that had at least one burst during the 5-minute recording, the following were calculated: mean burst duration, mean number of spikes per burst, mean spike frequency within the bursts, mean percentage of spikes within the bursts, mean number of bursts per minute, and mean interval between bursts. These values were then averaged for each slice; however, for the co-cultures, the averaging was only carried out if both of the slices had bursts, with the exception of the co-cultures that had not been placed contiguously. For the first set of experiments, there were six hippocampal slice cultures, six entorhinal slice cultures, and 12 co-cultures (six with the slices placed contiguously and six with the slices placed apart). For the second set of experiments, there were eight *WT* hippocampal slice cultures, seven *WT* entorhinal slice cultures, seven *WT* co-cultures, seven tau^{KO} hippocampal slice cultures, eight tau^{KO} entorhinal slice cultures, and six tau^{KO} co-cultures. Graphical representations of the extracellular neuronal activity (timestamps) were obtained using the Neuroexplorer software.

Time points	**4 DIV**	**6 DIV**	**8 DIV**	**10 DIV**
Hippocampal slice cultures	**5** 23.8 [11–40]	**6** 34.5 [22–52]	**6** 41.3 [23–54]	**6** 40.8 [19–55]
Entorhinal slice cultures	**6** 25.2 [8–39]	**6** 26.7 [8–41]	**6** 29.2 [9–45]	**6** 30.2 [7–46]
Co-cultures with the slices placed contiguously	**6** Hip 23.7 [2–36] Ent 14.8 [6–19]	**6** Hip 25.8 [3–38] Ent 15.8 [6–21]	**6** Hip 27 [4–38] Ent 16.5 [6–22]	**5** Hip 25.8 [5–38] Ent 17.0 [5–21]

Co-cultures with the slices placed ≥4 mm apart	**6** Ent 41.5 [36–46]	**5** Ent 43.4 [33–48]	**6** Ent 43.2 [28–49]	**6** Ent 45.2 [33–51]

Table 1: First set of experiments (from C57BL/6JRj mice): Total number of slice cultures included in the final analysis for each time point. The values in bold show the number of slice cultures included in the final analysis. The average number of active electrodes per slice is shown below these values, with the minimum and maximum number of active electrodes per slice shown in brackets.

Abbreviations: DIV: days *in vitro*; Hip: hippocampal; Ent: entorhinal

Time points	**3 DIV**	**4 DIV**	**6 DIV**	**8 DIV**	**10 DIV**	**12 DIV**	**14 DIV**
WT hippocampal slice cultures	**8** 35.1 [7–50]	**8** 32.4 [13–51]	**8** 36.0 [20–53]	**7** 43.7 [26–51]	**8** 35.4 [11–48]	**8** 35.1 [5–55]	**6** 30.8 [12–54]
WT entorhinal slice cultures	**7** 19.6 [10–30]	**7** 24.1 [15–31]	**7** 31.0 [19–38]	**7** 36.7 [23–50]	**7** 36.7 [25–50]	**7** 35.7 [21–47]	**7** 36.3 [19–48]
WT co-cultures (~150 µm apart)	**5** Hip 22.2 [17–28] Ent 9.0 [5–15]	**7** Hip 19.7 [9–33] Ent 14.6 [7–20]	**7** Hip 20.9 [11–32] Ent 16.7 [8–25]	**6** Hip 21.8 [15–33] Ent 17.0 [12–22]	**7** Hip 21.0 [14–33] Ent 16.9 [11–22]	**7** Hip 21.3 [12–33] Ent 16.6 [11–24]	**6** Hip 19.2 [10–33] Ent 15.8 [10–22]
KO hippocampal slice cultures	**7** 25.4 [8–40]	**7** 30.9 [9–43]	**7** 38.9 [15–54]	**7** 34.9 [18–48]	**7** 38.4 [22-48]	**7** 34.9 [26-46]	**7** 30.9 [19-45]
KO entorhinal slice cultures	**8** 16.4 [8–26]	**8** 23.1 [15–35]	**8** 34.5 [28–44]	**8** 38.4 [32–48]	**8** 41.0 [33–51]	**8** 42.0 [38–52]	**8** 42.2 [35–51]
KO co-cultures (~150 µm apart)	**6** Hip 14.2 [8–23] Ent 17.5 [12–23]	**6** Hip 16.7 [13–22] Ent 20.0 [16–23]	**6** Hip 18.0 [11–25] Ent 22.8 [18–29]	**6** Hip 19.3 [14–25] Ent 24.5 [21–28]	**5** Hip 18.8 [14–26] Ent 25.2 [22–29]	**5** Hip 18.8 [9–27] Ent 23.2 [16–29]	**4** Hip 18.3 [11–25] Ent 23.5 [14–29]

Table 2: Second set of experiments (from *WT* and *tau*^{KO} mice): Total number of slice cultures included in the final analysis for each time point. The values in bold show the number of slice cultures included in the final analysis. The average number of active electrodes per slice is shown below these values, with the minimum and maximum number of active electrodes per slice shown in brackets. Abbreviations: DIV: days *in vitro*; Hip: hippocampal; Ent: entorhinal; *KO*: *tau*^{KO} ; *WT*: *wild type*

182

183 **Analysis of the spike train synchrony**

184 The spike train synchrony was analyzed for all of the active electrodes on the condition that there were
185 at least five active electrodes in a slice. Different measures of synchrony were adopted in order to
186 analyze different aspects of the synchrony. These included time-scale independent measures, namely
187 the ARI-SPIKE-distance, the A-SPIKE-synchronization, the A-ISI-distance, the A-SPIKE-distance
188 (Satuvuori et al., 2017), and the Spike-contrast (Ciba et al., 2018); and time-scale dependent measures,
189 namely Selinger's measure (Selinger et al., 2004) and the spike time tiling coefficient (STTC; Cutts and
190 Eglen, 2014). The ARI-SPIKE-distance and A-SPIKE-distance both measure the accuracy of spike times,
191 with the former measure being independent of the spike rate and the latter measure varying according
192 to the spike rate. In contrast, the A-ISI-distance measures differences in the instantaneous spike rate
193 between spike trains. The ARI-SPIKE-distance, A-SPIKE-distance, and A-ISI-distance can be used to
194 assess synchrony by subtracting the distance value from one. The A-SPIKE-synchronization is a co-
195 incidence detector providing a measure of the similarity between spike trains. It is sensitive to the
196 number of spikes. The Spike-contrast was also included in the analyses, as it is highly robust against
197 erroneous spike trains (Ciba et al., 2020) and it provides information about the time scale of the
198 maximum synchrony (Ciba et al., 2018). All of these time-scale independent measures automatically
199 adapt their time scale to the data, which is useful for explorative studies where the time scale of the
200 data is unknown. We also adopted time-scale dependent measures, which are useful if only particular
201 time scales are relevant. The measures we adopted are robust against missing spikes or additional
202 spikes due to noise. As previous *in vitro* experiments using MEAs have shown that drug-induced
203 synchrony changes can be detected on time scales in the hundreds of milliseconds (Ciba et al., 2020;
204 Eisenman et al., 2015; Selinger et al., 2004), we adopted measures and selected parameters suited to
205 this time scale. We chose Selinger's measure, which is based on correlations between binned spike
206 trains (we set the bin size to 500 ms), and the STTC measure, which is spike-rate independent with a

time-window set at 100 ms (for this measure, spike A is considered to be in synchrony with spike B if it occurs within a time window of +/- 100 ms around spike B).

We obtained measures of both the intra-slice synchrony and the global synchrony, which refer to the synchrony within a slice or within a two-slice network, respectively. This involved calculating the synchrony between all of the spike train pairs and then averaging them to obtain a single value (with the exception of the Spike-contrast, which already returns a single value for all of the spike trains). The inter-slice synchrony was also calculated for the co-cultures. For this, the calculation only included the spike train pairs between the two slices; the remaining spike train pairs within each slice were excluded. In addition to the synchrony measures, the Spike-contrast also provided the time scale range (upper and lower time scales) that contained the highest amount of synchrony.

All of the measures were calculated using a customized Matlab-based toolbox called DrCell (https://github.com/biomemsLAB/DrCell).

Analysis of the connectivity and network topology

The connectivity was analyzed for all of the active electrodes on the condition that there were at least five active electrodes in a slice. The functional connectivity of the networks was estimated using the cross-correlation-based method, *Total Spiking Probability Edges* (TSPE); this was chosen based on its speed and high accuracy (De Blasi et al., 2019). The TSPE provided a measure of the estimated connectivity strength between each pair of spike trains, and it distinguished between excitatory (E) and inhibitory (I) connections. These pairwise values were stored in a matrix (connectivity matrix: CM) and values below a certain threshold were excluded. This threshold was determined based on the double threshold (DDT) method (Boschi et al., 2021), which provides greater precision than simple thresholding and less computation time than shuffling-based approaches. The parameter of DDT was set to 2, resulting in a final threshold of mean(CM) + 2* std(CM).

The estimated connectivity of the different cell cultures was normalized prior to carrying out statistical comparisons. This was necessary because the range of values was not limited. For this, we extracted the following relative features: Connection strength ratio (E/I), number of connections ratio (E/I), and second moment of the degree distribution (k^2).

The connectivity estimation was performed in Matlab using the code https://github.com/biomemsLAB/TSPE.

Statistics

Statistical analyses were carried out using the two-sided Wilcoxon-Mann-Whitney test (also known as the Wilcoxon rank-sum test).

RESULTS

In *WT* hippocampal-entorhinal slice co-cultures, the burst activity of the entorhinal slice decreased

In a first set of experiments (from C57BL/6JR mice) we examined whether the spontaneous neuronal activity in the hippocampal and entorhinal brain slices was significantly different when they were cultured separately or together (**Figure 1**). It was found that both the single-slice cultures and the co-cultures (**Figure 1A-D**) generated synchronized burst firing, as previously described for slice cultures prepared from different brain regions (Chu et al., 2012; Dossi et al., 2013; Hofmann et al., 2004). Analyses were carried out for the different burst parameters: mean number of bursts per minute, mean burst duration, and mean number of spikes per burst. Differences were found between the hippocampal and entorhinal slices cultured alone (**Figure 1E** and **Supplementary figure 1**), as expected for slices prepared from different brain regions. For the co-cultures with the slices placed contiguously, the hippocampal and entorhinal slices were found to have synchronized spontaneous neuronal activity (**Figure 1I**), thus demonstrating that functional connections had formed between them. The burst

parameters were found to be similar in the hippocampal slices, whether they were cultured alone or alongside the entorhinal slices (**Figure 1F** and **Supplementary figure 1**). However, for the entorhinal slices, the number of bursts per minute was lower from 8 DIV (days *in vitro*) when they were cultured beside the hippocampal slices, as opposed to alone (**Figure 1G**). When the hippocampal slices were placed at a distance from the entorhinal slices in the co-cultures (**Figure 1D**) resulting in fewer connections forming between the slices, no significant differences were observed (**Figure 1H**). This indicates that in *WT* co-cultures, the hippocampal slice affects the entorhinal activity by means of connections that are formed between the slices.

In the second set of experiments, we investigated the role of tau in neural networks by comparing the neuronal activity in slices prepared from tau^{KO} and *WT* littermates (**Supplementary figure 2**). This included hippocampal and entorhinal single-slice cultures (one-slice networks) and hippocampal-entorhinal co-cultures (two-slice networks). For these experiments, the spontaneous neuronal activity was recorded over two weeks.

Large differences between the spontaneous burst activity of hippocampal and entorhinal one-slice networks

For the hippocampal and entorhinal single-slice cultures, it was found that there was little difference in the burst parameters for the first days of culture, but that large differences emerged after about one week for both the *WT* and tau^{KO} slices (**Figure 2** and **Supplementary figure 3**). For both genotypes, the average burst duration, the number of spikes per burst, and the percentage of spikes within the bursts were all significantly higher in the entorhinal slices (**Figure 2**). The average number of bursts per minute was also significantly higher in the entorhinal slices at 12 and 14 DIV for both genotypes, and a tendency (p-value < 0.1) could be observed at 6 and 8 DIV for the *WT* and tau^{KO} cultures, respectively (**Figure 2** and **Supplementary figure 3**). Of note, the difference in burst frequency between the entorhinal and hippocampal slices occurred more rapidly in the first set of experiments; this could be attributed to differences in the slice preparation (P5 instead of P7). In the second set of experiments,

it was also found that the average interval between bursts was significantly longer in the hippocampal slices at certain time points (**Figure 2**). The only measure that differed significantly between the hippocampal and entorhinal single-slice cultures as early as 3 DIV was the spike frequency within bursts; this difference was only found in the *WT* cultures, although the difference was also observed at 6 DIV in the *tau*^{KO} cultures (**Figure 2**).

No robust differences in the spontaneous burst activity of *WT* and *tau*^{KO} one-slice networks

For the entorhinal single-slice cultures, there was a slightly lower number of spikes per burst in the *tau*^{KO} cultures compared with the *WT* cultures at 8 DIV (**Figure 3A**), with a tendency also observed at 10 DIV (*p*-value = 0.054; **Supplementary figure 4A**). For the hippocampal single-slice cultures, the number of spikes per burst and the spike frequency within the bursts was lower in the *tau*^{KO} cultures compared with the *WT* cultures at 3 DIV (**Figure 3B** and **Supplementary figure 4D**). As all of the differences found were only apparent for one of the DIV, we were not able to conclude that there are consistent differences between *WT* and *tau*^{KO} one-slice networks.

Decreased burst activity in the entorhinal slice of the *tau*^{KO} co-cultures, but later than in the *WT* co-cultures

The spontaneous neuronal activity in the hippocampal and entorhinal slices was synchronized, both in the *WT* and *tau*^{KO} co-cultures (**Supplementary figure 5**). This indicates that functional connections were formed between the co-cultured slices, resulting in a two-slice functional network. Based on our first set of experiments (**Figure 1**), we expected to find a decrease in the spontaneous burst activity of the entorhinal slice in the co-cultures. However, as previous studies have shown that tau is involved in neurite growth, we reasoned that the *tau*^{KO} co-cultures may have impaired and/or delayed formation of inter-slice connections. This could conceivably lead to reduced and/or postponed effects on the entorhinal slice. In line with this, we found that the *WT* co-cultures had a significantly reduced burst duration and number of spikes per burst in the entorhinal slices at 10 and 12 DIV compared with *WT*

entorhinal single-slice cultures (**Figure 3C**), whereas this was not found in the *tau*^{KO} co-cultures (**Figure 3D**). There was even a slight, significant increase in the number of spikes per burst at 8 DIV in the *tau*^{KO} co-cultured entorhinal slices. However, by 14 DIV, both genotypes had a significantly reduced number of bursts per minute in the entorhinal slices in co-culture conditions (**Figure 3C-D** and **Supplementary figure 4B-C**). Of note, this reduction in the number of bursts may possibly relate to a decrease in the number of spikes per burst, as a certain number of spikes were required to identify bursts. Overall, it can be seen that in *tau*^{KO} co-cultures, the hippocampal slice still decreases the burst activity of the entorhinal slice, but this is delayed and/or less pronounced than in *WT* co-cultures. Regarding a reciprocal effect of the entorhinal slice on the hippocampal slice, the only effect we observed was a one-off increase in the number of bursts per minute at 8 DIV in the *tau*^{KO} co-cultures (**Figure 3E-F** and **Supplementary figure 4E-F**).

Tau ablation has a late anti-synchrony effect on the hippocampal-entorhinal two-slice network

We assessed whether the formation of inter-slice connections was delayed in *tau*^{KO} co-cultures by measuring the neuronal synchrony over time in both the *WT* and *tau*^{KO} co-cultures (Hofmann et al., 2004). For this, we determined the inter-slice synchrony, which reflects the functional connections between the slices. As there are a number of different algorithms for evaluating synchrony, we adopted several different measures: A-SPIKE-synchronization, Spike-contrast, ARI-SPIKE-distance, A-ISI-distance, A-SPIKE-distance, Selinger's method, and the spike time tiling coefficient (STTC; see 'Method' section for more details; **Figure 4A** and **Supplementary figure 6A**). We found that the loss of tau did not affect the evolution of the inter-slice synchrony over the first week of co-culture. This indicates that there was no initial delay in the formation of inter-slice connections in the *tau*^{KO} co-cultures. For the second week of co-culture, we found that two measures revealed lower inter-slice synchrony in the *tau*^{KO} co-cultures at 12 DIV; this was also found for one measure at 14 DIV (**Figure 4A**). In addition, the Spike-contrast method revealed that the maximum inter-slice synchrony occurred at a larger time scale in the *WT* co-cultures at 8 and 10 DIV (**Supplementary figure 7**), which reflects

longer periods of signal and/or silence. Together, these results indicate that tau ablation affects the connections between the hippocampal and entorhinal slices in the second week of co-culture.

We carried out further analyses to determine whether tau ablation only affects the inter-slice connections or whether it affects the hippocampal-entorhinal co-cultures in a more general way. For this, we estimated the global synchrony within the *WT* and *tau^{KO}* co-cultures using the same measures of synchrony listed above (**Figure 4B** and **Supplementary figure 6B**). We found that all but one measure revealed a lower global synchrony in the *tau^{KO}* two-slice networks at 10, 12, and/or 14 DIV. Importantly, there was no corresponding synchrony decrease in the *tau^{KO}* single-slice cultures at any time point for any of the measures (**Figure 4C-D** and **Supplementary figure 8**). Indeed, there were even one-off synchrony increases in the *tau^{KO}* hippocampal single-slice cultures, as shown by two measures (**Figure 4C**). These results indicate that (1) tau ablation induces an alternative remodeling of the hippocampal-entorhinal two-slice network, leading to an anti-synchrony effect at later stages, and (2) the effect is specific to co-cultures.

Tau ablation does not consistently modify the neural network topology in either the single-slice cultures or the co-cultures

We performed a connectivity analysis to gain greater insight into how tau ablation decreases synchrony in the two-slice network during the second week of co-culture. For this, we adopted the *Total Spiking Probability Edges* (TSPE) method (De Blasi et al., 2019) to estimate the functional connectivity within the *WT* and *tau^{KO}* two-slice networks. This method provided an estimate of the connection strength between electrodes, and it distinguished between excitatory and inhibitory connections. Connectivity network graphs were generated for the *WT* and *tau^{KO}* co-cultures (examples are presented in **Figure 5A, B**), and the E/I number and strength ratios were extracted and compared (**Figure 5C, top** and **Supplementary figure 9A-B**). It was found that the *tau^{KO}* co-cultures had a higher E/I number ratio at 3DIV but lower E/I number and strength ratios at 12 DIV. The E/I number and strength ratios of the inter-slice connections were compared between the *WT* and *tau^{KO}* co-cultures

(**Figure 5D-E** and **Supplementary figure 9E-H**) and revealed that both ratios were lower in the *tau*^{KO} hippocampal-to-entorhinal connections at 12 DIV (**Figure 5D**), whereas there were no differences for the entorhinal-to-hippocampal connections (**Figure 5E**). Thus, at 12 DIV, there was a transitory reduction in the E/I ratios both globally and in the hippocampal-to-entorhinal connections for the *tau*^{KO} two-slice networks (**Figure 5C-D**).

Connectivity analyses were also performed for the single-slice cultures. Only one difference was found for the *tau*^{KO} hippocampal single-slice cultures: the E/I strength ratio increased at 8 DIV compared with *WT* slices (**Figure 5F, top** and **Supplementary figure 10A, top**). For the *tau*^{KO} entorhinal slices, the E/I ratios were not found to alter (**Figure 5G, top** and **Supplementary figure 10B, top**). These findings indicate that tau ablation does not have a universal effect on the E/I balance of neural networks.

We examined another parameter that is important for network synchrony, namely homogeneity in the distribution of connectivity. Previous work using theoretical models has shown that homogeneity promotes network synchrony (Nishikawa et al., 2003). To examine this, we extracted the second moment of the connectivity distribution (k^2) for the excitatory and inhibitory connections. These were then compared between the *WT* and *tau*^{KO} cultures. It was found that there were no significant differences in k^2 between the *WT* and *tau*^{KO} two-slice networks, irrespective of the type of connection (**Figure 5C, bottom** and **Supplementary figure 9C-D**). There were also no differences for the single-slice cultures (**Figure 5F-G, bottom** and **Supplementary figure 10A-B, bottom**).

Tau ablation has differential effects on the hippocampal and entorhinal sub-networks in co-culture

Our data indicated that tau ablation leads to an anti-synchrony effect that is specific to the co-cultures, as this effect was not observed in the single-slice cultures (**Figure 4C-D**). Although our connectivity analysis revealed consistent changes in the co-cultures, this was only at 12DIV (**Figure 5C-D**), whereas the anti-synchrony effect was longer than this. We considered whether tau ablation could lead to

subtle modifications and/or alternative remodeling of the two-slice network. Analyses at the global level may not be able to reveal such subtle differences, as they may be partially masked. We therefore examined differences between the single-slice cultures and the corresponding sub-networks in co-culture, both for the *WT* and *tau*^{KO} genotypes. The different measures of synchrony were used, as above, to compare the intra-slice synchrony between single-slice and co-culture conditions (**Figures 6A-B** and **7A-B** and **Supplementary figures 11** and **12**). The results showed that the hippocampal synchrony consistently increased over time in the *WT* co-cultures compared with the single-slice cultures; this was found for all but one of the measures (**Figure 6A**). In contrast, there was no synchrony increase in the *tau*^{KO} hippocampal slices in co-culture for any of the measures; indeed, the hippocampal synchrony even decreased at 3 DIV for two of the measures (**Figure 6B**). For the entorhinal slices, the synchrony was not found to increase over the first week for the *WT* co-cultures compared with the single-slice cultures (**Figure 7A**; note that the synchrony decreased at 3 DIV for one of the measures). In contrast, the entorhinal synchrony was found to consistently increase over the first week in the *tau*^{KO} co-cultures; this was found for all but one of the measures (**Figure 7B**). However, at a later time-point (12 DIV), the entorhinal synchrony increased in the *WT* co-cultures compared with the single-slice cultures, as revealed by three of the measures (**Figure 7A**), whereas there was no increase of the entorhinal synchrony in the *tau*^{KO} co-cultures (**Figure 7B**; note that the synchrony decreased according to one measure).

To summarize, we found that in the *WT* hippocampal-entorhinal co-cultures, the hippocampal synchrony consistently increased over almost all of the time points compared with the single-slice cultures. In contrast, the entorhinal synchrony stagnated towards the beginning of the co-culture, and finally increased towards the end compared with the single-slice cultures. This pattern was almost completely reversed in the absence of tau. Specifically, for the *tau*^{KO} co-cultures, it was found that the hippocampal synchrony decreased at the beginning of the co-culture and then remained fairly constant compared with the single-slice cultures. In contrast, the entorhinal synchrony consistently increased throughout the first week of co-culture and then stagnated towards the end. Taken together, our

results indicate that tau ablation has a global anti-synchrony effect on the hippocampal-entorhinal two-slice networks at later stages. However, when the evolution of the sub-networks in co-culture conditions are considered separately and compared with the single-slice cultures, the tau ablation can be seen to have an anti-synchrony effect on the hippocampal slice and a pro-synchrony effect on the entorhinal slice over the first week of co-culture.

Tau ablation reinforces E/I ratio reduction in the hippocampal sub-network of the co-cultures, and homogeneization of the distribution of connectivity in the entorhinal sub-network

The differential evolution of the intra-slice synchrony within the *WT* and *tau^{KO}* co-cultures, compared with the single-slice cultures, was unexpected. The findings revealed that tau ablation had opposite effects on the hippocampal and entorhinal slices in co-culture, which were anti-synchrony and pro-synchrony, respectively. We carried out additional analyses to further characterize how tau affects the evolution of synchrony within one and two-slice networks. For this, we resumed the connectivity analysis conducted previously, but we focused on the differences between the single-slice cultures and co-cultures, in *WT* and *tau^{KO}* contexts (**Figures 6C-D** and **7C-D** and **Supplementary figures 13** and **14**). We first compared the E/I ratios for the one-slice and two-slice networks. For the *tau^{KO}* hippocampal slices, we found that the E/I number ratio was significantly lower in the co-cultures at 6, 10, and 12 DIV. For the *WT* hippocampal slices, the E/I number ratio was also significantly lower in the co-cultures, but only at 6 DIV (**Figure 6C-D, top**). Concerning the E/I strength ratio, the *tau^{KO}* hippocampal slices had significantly lower ratios in the co-cultures at 8 DIV (**Figure 6D, top**), but there were no differences for the *WT* hippocampal slices. These results indicate that the co-culture conditions led to a stronger reduction in the E/I balance in the *tau^{KO}* hippocampal slices than in the *WT* slices.

For the entorhinal slices, we found that the E/I ratios did not significantly change in *tau^{KO}* co-cultures (**Figure 7 D, top**) and the E/I number ratio significantly increased at 6 DIV in *WT* co-cultures (**Figure 7C, top**).

We also carried out further analyses based on k^2 for the excitatory and inhibitory connections because of the link between network synchrony and network homogeneity. Of note, a high k^2 indicates a heterogeneous distribution of connectivity, while a low k^2 indicates a homogeneous distribution of connectivity; the latter has been shown to promote network synchrony. For the hippocampal slices, the k^2 punctually decreased in the co-cultures about half-way through the culture period; the reduction for the *WT* and *tau*^{KO} slices were comparable (**Figure 6C-D, bottom**). For the entorhinal slices, the k^2 was markedly lower in the *tau*^{KO} co-cultures than in the *tau*^{KO} single-slice cultures during the first week; this was the case for both the excitatory (3 and 4 DIV) and inhibitory connections (3, 4, and 6 DIV; **Figure 7D, bottom**). For the *WT* cultures, there was also a lower k^2 for the entorhinal slices in co-culture, but this was less pronounced (only significant at 4 DIV for the excitatory connections; **Figure 7C, bottom**). This indicates that in the absence of tau, there is a greater decrease in the heterogeneity of the connectivity distribution in entorhinal slices in co-culture compared with the single-slice cultures.

DISCUSSION

In this study, we adopted a new methodology designed to explore the role of particular genes/proteins in neural networks. This involved comparing the spontaneous extracellular neuronal activity of brain single-slice cultures and co-cultures (**Figure 8**). We used this method to explore how tau affects neural networks, which is important given its involvement in tauopathies and epilepsy. We focused on endogenous tau and so explored differences between *WT* and tau-depleted networks.

We first analyzed the burst firing in brain slices from *WT* and *tau*^{KO} mice. We found large, consistent differences between the hippocampal and entorhinal single-slice cultures, as expected for different brain regions. Specifically, we found that the extracellular activity in the entorhinal slices tended to increase over time so that it was higher than in the hippocampal slices. This was found to occur

irrespective of whether tau was expressed or not (**Figure 2**). When the *WT* and *tau*^{KO} single-slice cultures were compared, there were only a few, one-off differences, most notably a decrease in the number of spikes per burst in the absence of tau (**Figure 3A-B**). These observations are in line with previous work on *tau*^{KO} mice (Chang et al., 2021). However, as we did not adjust the alpha level (significance threshold) for multiple comparisons, such one-off differences should be interpreted with caution.

Analyses were run to assess the synchrony (**Figure 4C-D**) and connectivity (**Figure 5F-G**) in the single-slice cultures. These yielded similar results to the burst analyses, with just a few one-off differences. We reasoned that the analyses may have been too limited to reveal the effects of tau, because tau ablation may lead to very subtle phenotype differences in single-slice cultures. To address this, one possibility would be to increase the sample size so that even small phenotype differences would become apparent. However, we adopted another solution, which involved studying co-cultured brain slices. These form functional connections and undergo remodeling to create two-slice networks. We reasoned that the effects of tau ablation may become apparent within this context.

We used hippocampal-entorhinal brain slice co-cultures. We found that in the *WT* co-cultures, the number of bursts, the burst duration, and/or the number of spikes per burst were significantly lower in the entorhinal slices compared to when cultured alone (**Figures 1G and 3C**). This decreased activity was presumably due to the establishment of a two-slice network rather than to substances secreted by the hippocampal slice, as no effect was observed when the slices were co-cultured apart (**Figure 1H**). In the *tau*^{KO} co-cultures, reduced burst activity was also apparent in the entorhinal slices, but this occurred later than in the *WT* slices (**Figures 3C-D**). This could be attributed to tau ablation delaying the formation of functional connections between the brain slices. Alternatively, the remodeling processes involved in forming a two-slice network may have been altered by the absence of tau.

We investigated the synchronization or correlation of the activity in the co-cultured slices, as this may reflect the growth of functional inter-slice connections (**Figure 1I and supplementary figure 5**). We found that the inter-slice synchrony was similar in the *WT* co-cultures and *tau*^{KO} counterparts until 10

DIV (**Figure 4A**). This indicates that there is not an initial delay in the establishment of functional inter-slice connections in the absence of tau. However, towards the end of the co-culture, the inter-slice synchrony decreased in the *tau*^{KO} co-cultures (**Figure 4A**), and the *WT* co-cultures exhibited longer periods of activity and/or silence at 8 and 10 DIV (**Supplementary figure 7**). These data suggest that the two-slice network in the co-culture was somehow modified by the absence of tau. Further evidence for this was obtained by analyzing the global synchrony in the two-slice networks, where a late decrease was found in the *tau*^{KO} networks (**Figure 4B**). Altogether, these results suggest that tau ablation leads to a late anti-synchrony effect in the two-slice networks due to alternative network remodeling.

To further explore the possibility that tau ablation leads to alternative network remodeling, we carried out a connectivity analysis for the *WT* and *tau*^{KO} co-cultures (**Figure 5A-C**). It has to be noted that the TSPE method has only been evaluated using simulated data with characteristics of *in vivo* networks, and hence, would possibly benefit from being optimized for *ex vivo* networks. Only a few one-off differences were found, including a reduction in the estimated E/I number and strength ratios at 12 DIV for the *tau*^{KO} co-cultures. This observation is in line with previous work indicating that tau ablation reduces hypersynchrony by lowering the E/I ratio (Chang et al., 2021).

We were concerned that global comparisons between *WT* and *tau*^{KO} co-cultures could potentially mask subtle differences between the two-slice networks. We therefore carried out further analyses to examine the evolution of the synchrony within single-slice and co-cultures (**Figures 6A-B and 7A-B**). For the *WT* slices, we found that the hippocampal synchrony consistently increased over time in the co-cultures compared with the single-slice cultures (**Figure 6A**). This was not found for the *tau*^{KO} slices, where there was even a decrease in the hippocampal synchrony at the beginning of the co-culture according to certain measures (**Figure 6B**). The entorhinal synchrony was found similar in the *WT* co-cultures compared to the single-slice cultures at the beginning of the culture period, but it increased towards the end (**Figure 7A**). In the absence of tau, the entorhinal synchrony consistently increased

over the first week of co-culture (**Figure 7B**) and then stagnated, possibly even decreasing towards the end of the co-culture (**Figure 7B**). Altogether, these results indicate that (a) the synchrony of the hippocampal and entorhinal sub-networks evolve differently over time when in co-culture, and (b) tau ablation modifies these patterns. More precisely, tau ablation appears to have an anti-synchrony effect on the hippocampal sub-network and an early pro-synchrony effect on the entorhinal sub-network.

Previous work has shown that tau ablation (*tau*^{KO}) protects against network hypersynchrony in primary hippocampal neurons (Chang et al., 2021). This finding was attributed to a reduction in the E/I ratio at the level of cells (Chang et al., 2021), although it is relevant to note that the experimental conditions were very artificial (KCl treatment). Protective effects due to tau ablation have also been found in AD transgenic mice (double transgenic *humanAPPJ9/Fyn* mice; Roberson et al., 2011), which were attributed to the same mechanism. In our study, the experimental design was different, as it involved connecting different brain-slice networks. Nevertheless, we found that there was a decrease in the E/I number ratio over several days in the hippocampal slices of the *tau*^{KO} co-cultures compared with the single-slice cultures, whereas a prolonged effect was not observed in the *WT* co-cultures (**Figure 6C-D, top**). We therefore concluded that the anti-synchrony effect attributed to tau reduction in the hippocampal co-cultured slices also appeared to be associated with a decrease in the E/I ratios. However, it is relevant to note that E/I ratio reduction was not observed in the entorhinal slice in co-culture. We hypothesize that this is because tau ablation differentially affects the remodeling of distinct *ex vivo* sub-networks according to their topology. This would be in line with findings that tau ablation has different effects on excitatory and inhibitory neurons both *in vitro* and *in vivo* (Chang et al., 2021; Shao et al., 2022).

We examined the k^2 in the co-cultured slices, as work on network theory indicates that homogeneous connectivity promotes network synchrony (Nishikawa et al., 2003). There is evidence in support of this, such as a study by Khambhati and colleagues, which examined functional networks recreated from intracranial electrophysiological recordings from epileptic patients having seizure events (Khambhati

et al., 2016). They compared the functional networks for seizures that remained focal with those that spread throughout the brain, and found a strong negative correlation between the network heterogeneity and the network synchronizability. In our study, we found that the connectivity distribution was considerably more homogeneous in the entorhinal slices of the *tau*^{KO} co-cultures compared with the single-slice cultures during the first week (**Figure 7D, bottom**). For the *WT* cultures, this difference could also be seen but it was less marked (**Figure 7C, bottom**). Thus, we hypothesized that the increased homogeneity in the co-cultured *tau*^{KO} entorhinal slices could account for the pro-synchrony effect that was observed (**Figure 7B**). It is relevant to note that the connectivity distribution within both the *WT* and *tau*^{KO} entorhinal single-slice cultures tended to homogenize over time (**Supplementary figure 10B**). This could be due to *ex vivo* rewiring processes within the entorhinal slices. Given that tau is involved in neurite outgrowth, tau ablation would presumably affect this process and, possibly, would potentiate entorhinal network homogenization in co-culture.

It could be argued that our study could not conclude that tau ablation has anti-synchrony/pro-synchrony effects on different slices in co-culture by direct comparisons between *WT* and *tau*^{KO} co-cultures. Actually, the results were in line with differences found between the single-slice and co-culture conditions, although these were less marked (**Figure 9** and **Supplementary figure 15**). As the hippocampal synchrony in the *tau*^{KO} co-cultures compared with the *WT* co-cultures was found to be significantly lower over several time points, this supports there being an anti-synchrony effect within the hippocampal sub-network. In contrast, the entorhinal synchrony in the *tau*^{KO} co-cultures was found to be significantly higher at 3 DIV, thus supporting an early pro-synchrony effect within the entorhinal sub-network. We were not able to observe other effects induced by tau ablation by comparing directly the co-cultures. This may be because comparisons between the single-slice cultures and co-cultures in *WT* and *tau*^{KO} contexts are more powerful with less effect of masking.

Lastly, it is of interest to consider the entorhinal synchrony differences between the single-slice cultures and the co-cultures. Here, we found that the synchrony increased in the *WT* co-cultures at 12

DIV, while it possibly decreased in the *tau*^{KO} co-cultures. This indicates that tau ablation may have an anti-synchrony effect on the entorhinal slice as well as the hippocampal slice in co-culture at 12 DIV. This would explain why global connectivity differences are only found at 12 DIV between the *WT* and *tau*^{KO} two-slice networks.

CONCLUSION

We found that tau ablation reduced the synchrony in the hippocampal/entorhinal two-slice network at later stages of the co-culture. There were differential effects of tau ablation at the sub-network scale, including (1) an anti-synchrony effect within the hippocampal sub-network throughout the culture period, which possibly resulted from a reduction in the E/I ratio, and (2) a pro-synchrony effect within the entorhinal sub-network at early stages. It is possible that this latter effect may be due to tau ablation promoting an accelerated homogenization of the connectivity distribution in the entorhinal sub-network. The different effects of tau ablation are likely to depend upon the sub-network topology.

The new *in vitro* methodology presented here (**Figure 8**) can reveal the effects of genes/proteins on the network remodeling that occurs in brain slice co-cultures. This complements the classical pharmacological approach for exploring the functions of genes/proteins in brain networks, and it has two great strengths. Firstly, it combines analysis of the burst parameters, synchrony, and connectivity. This increases its power to detect subtle effects. Secondly, the method could be used to study a wide range of physiologically-relevant networks, as organotypic slice cultures can prepared from a wide range of brain regions.

Acknowledgements: This work was supported by the LabEx DISTALZ, the I-SITE ULNE foundation (Re-SpecT project), the Agence National pour la Recherche (NanoIntra project) and the Joint Inserm-Uni-

583 versity Chairs program. The authors thank the animal care staff of the EOPS facility (UMS-2014 US41
584 PLBS).

585

586 **FIGURES**

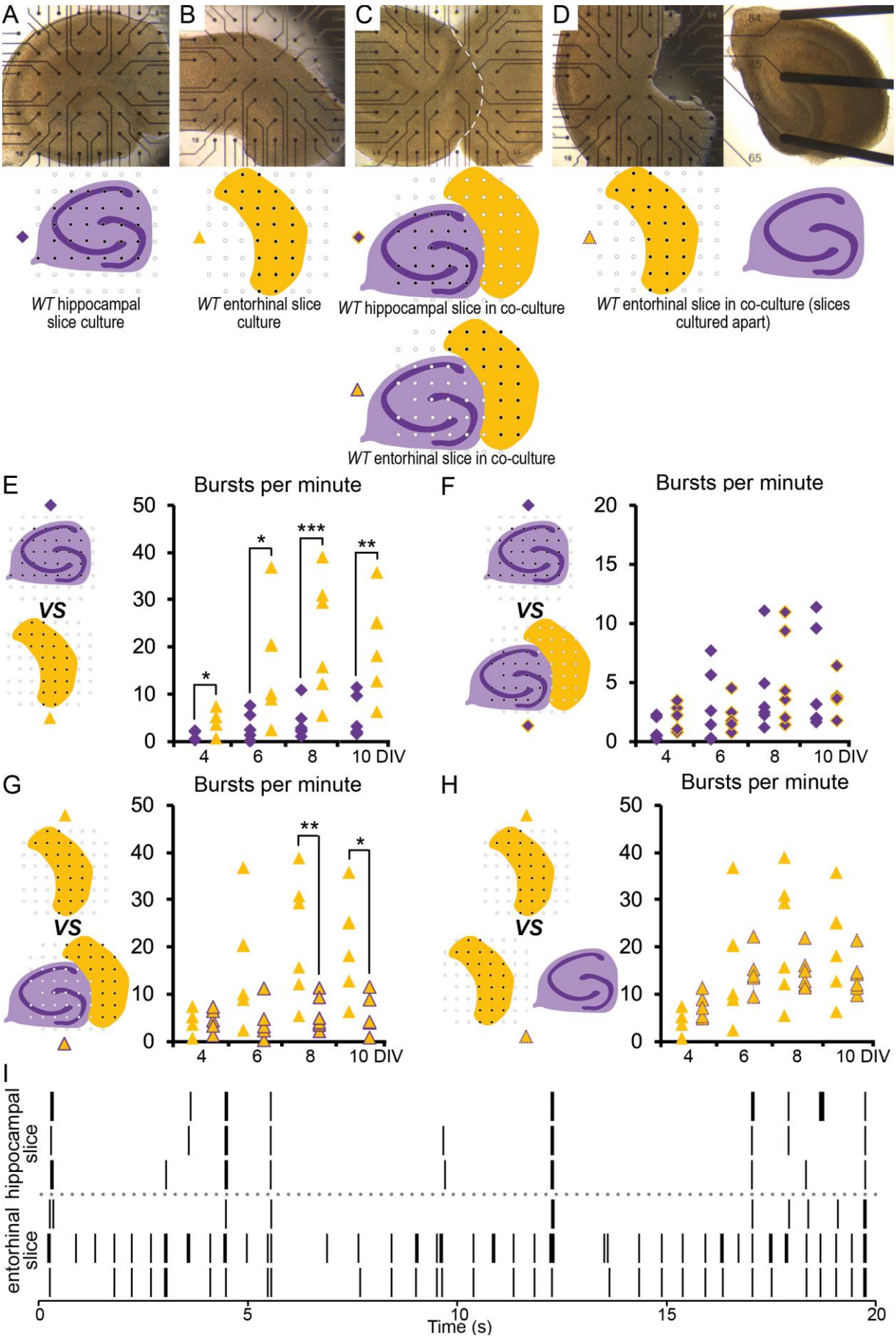
A
B
C
D
WT hippocampal slice culture
WT entorhinal slice culture
WT hippocampal slice in co-culture
WT entorhinal slice in co-culture
WT entorhinal slice in co-culture (slices cultured apart)
E
Bursts per minute
VS
F
Bursts per minute
VS
G
Bursts per minute
VS
H
Bursts per minute
VS
I
hippocampal slice
entorhinal slice
Time (s)
4
6
8
10 DIV

587

Figure 1: In *WT* hippocampal-entorhinal co-cultures, the spontaneous burst activity of the entorhinal slice was lower than in entorhinal slices cultured alone.

(A-D) Representative images of *WT* hippocampal (A) and entorhinal (B) single-slice cultures and co-cultures (C, D) on micro-electrode arrays (images acquired after plating). In the co-cultures, the hippocampal slice was either positioned contiguous to the entorhinal slice (C) or at a distance (D). The diagrams show the electrode configuration (in black) that was analyzed for each condition.

(E-H) Mean number of bursts per minute for each condition over 10 days. Comparisons are shown between the hippocampal (purple) and entorhinal (orange) single-slice cultures (E), between the hippocampal single-slice cultures (purple) and the hippocampal slices in co-culture (purple circled in orange) (F), between the entorhinal single-slice cultures (orange) and the entorhinal slices in co-culture (orange circled in purple) (G), and between the entorhinal single-slice cultures (orange) and the entorhinal slices in co-cultures positioned at a distance (in orange circled in dashed purple) (H). The means were obtained using all of the electrodes that exhibited burst firing within each culture. *: p-value < 0.05, **: p-value < 0.01, and ***: p-value < 0.005 (Wilcoxon-Mann-Whitney test).

(I) Representative timestamps extracted from 20-second-long electrode recordings from the hippocampus (top) and the entorhinal cortex (bottom); the recordings were from a *WT* co-culture, such as the one shown in (C), after 8 days *in vitro* (DIV). Each vertical line represents a spike.

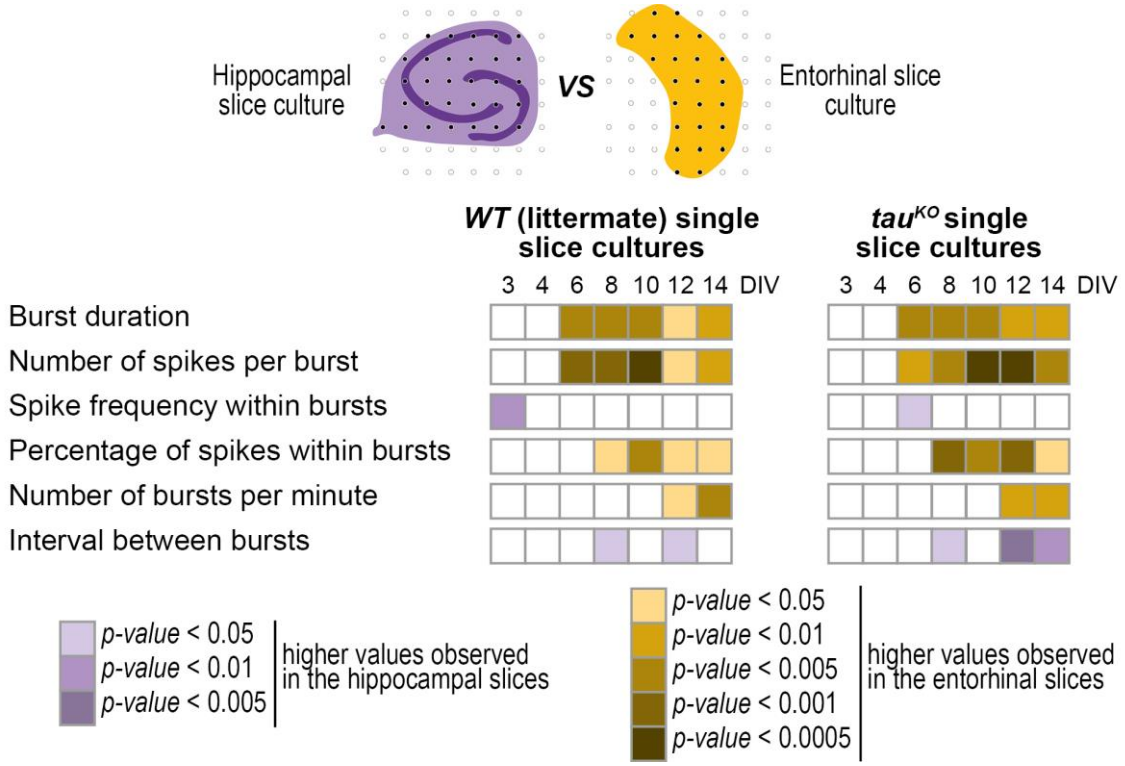

606

607 **Figure 2: Hippocampal and entorhinal single-slice cultures exhibited spontaneous burst activity with**

608 **distinct characteristics, irrespective of the tau status.**

609 Measures of the burst activity over two weeks for the hippocampal and entorhinal single-slice cultures

610 from *wt* (left) or *tau*^{KO} (right) mice. The extracellular recordings were obtained from *wt* or *tau*^{KO}

611 hippocampal and entorhinal single slices that were cultured on micro-electrode arrays; the recordings

612 were obtained at 3 days *in vitro* (DIV) and then every second day from 4 DIV to 14 DIV. The mean burst

613 duration, number of spikes per burst, spike frequency, percentage of spikes within bursts, number of

614 bursts per minute, and the interval between bursts were extracted and compared for each time point.

615 The shades of purple or orange/ochre indicate significantly higher values for the hippocampal or

616 entorhinal slices, respectively, with the *p*-values shown by the color intensity, ranging from 0.05 to

617 0.0005 (Wilcoxon-Mann-Whitney test).

618

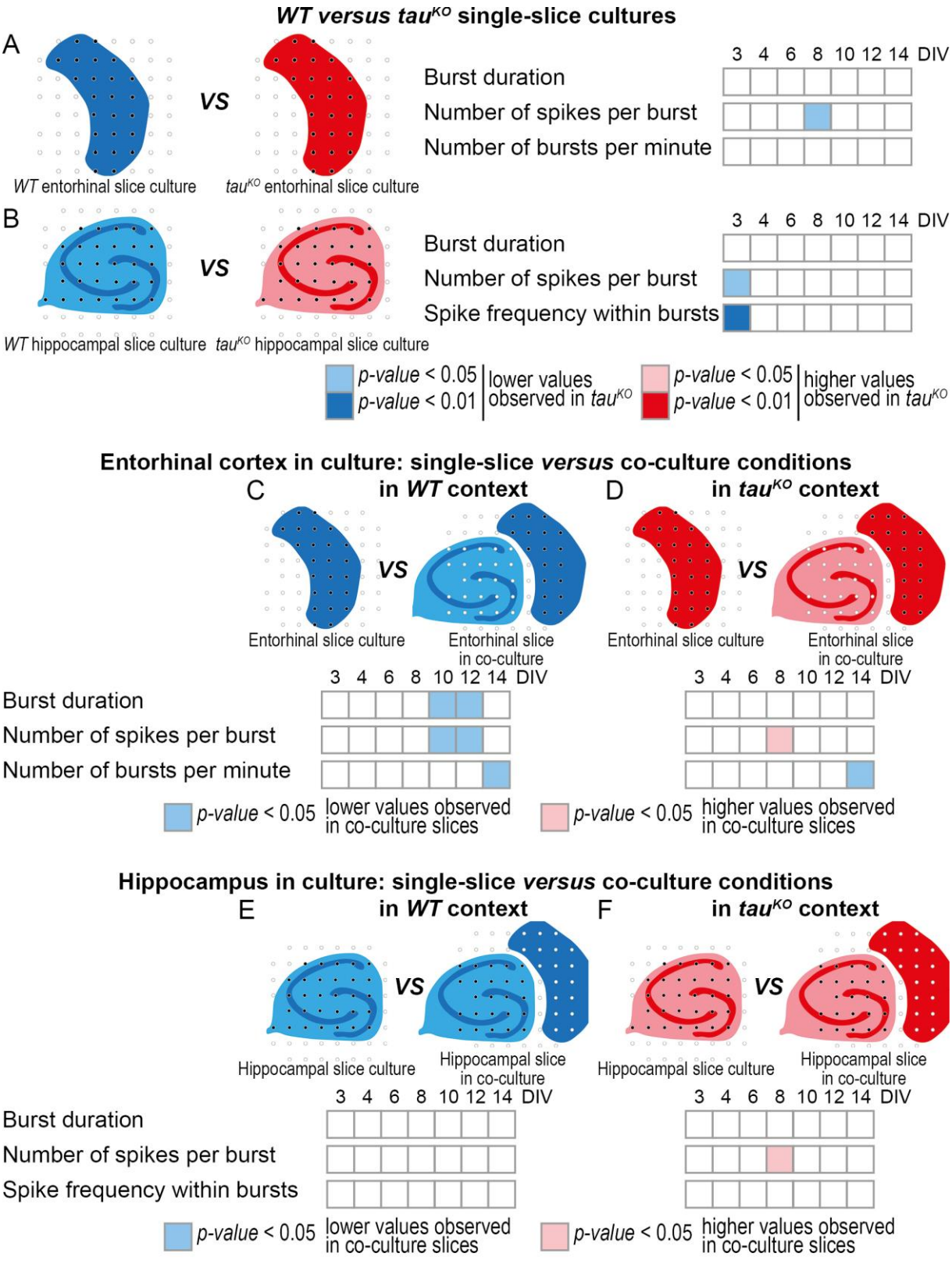

Figure 3: In *tau*^{KO} hippocampal-entorhinal co-cultures, the spontaneous burst activity in the entorhinal slice decreased in a delayed fashion compared with *WT* co-cultures.

622 Measures of the burst activity over two weeks for the *WT* (blue) and *tau*^{KO} (red) entorhinal (A, C-D) and
623 hippocampal (B, E-F) slices in the single-slice cultures and co-cultures. The diagrams indicate the
624 conditions that were compared and the electrode configuration that was analyzed (in black).
625 (A, C-D) The mean burst duration, number of spikes per burst, and number of bursts per minute were
626 extracted from the extracellular recordings. For each time point, these values were compared between
627 the *WT* and *tau*^{KO} entorhinal single-slice cultures (A), between the *WT* entorhinal single-slice cultures
628 and the *WT* entorhinal slices in co-culture (C), and between the *tau*^{KO} entorhinal single-slice cultures
629 and the *tau*^{KO} entorhinal slices in co-culture (D).
630 (B, E-F) The mean burst duration, number of spikes per burst, and spike frequency within bursts were
631 extracted from the extracellular recordings. For each time point, these were compared between the
632 *WT* and *tau*^{KO} hippocampal single-slice cultures (B), between the *WT* hippocampal single-slice cultures
633 and the *WT* hippocampal slices in co-culture (E), and between the *tau*^{KO} hippocampal single-slice
634 cultures and the *tau*^{KO} hippocampal slices in co-culture (F).
635 (A-B) The shades of blue indicate significantly lower values for the *tau*^{KO} slices and the shades of pink
636 indicate significantly higher values for the *tau*^{KO} slices. The *p*-values are indicated by the color intensity,
637 ranging from 0.05 to 0.01 (Wilcoxon-Mann-Whitney test).
638 (C-F) Blue indicates significantly lower values for the co-cultured slices and pink indicates significantly
639 higher values for the co-cultured slices with a p-value < 0.05 (Wilcoxon-Mann-Whitney test).
640

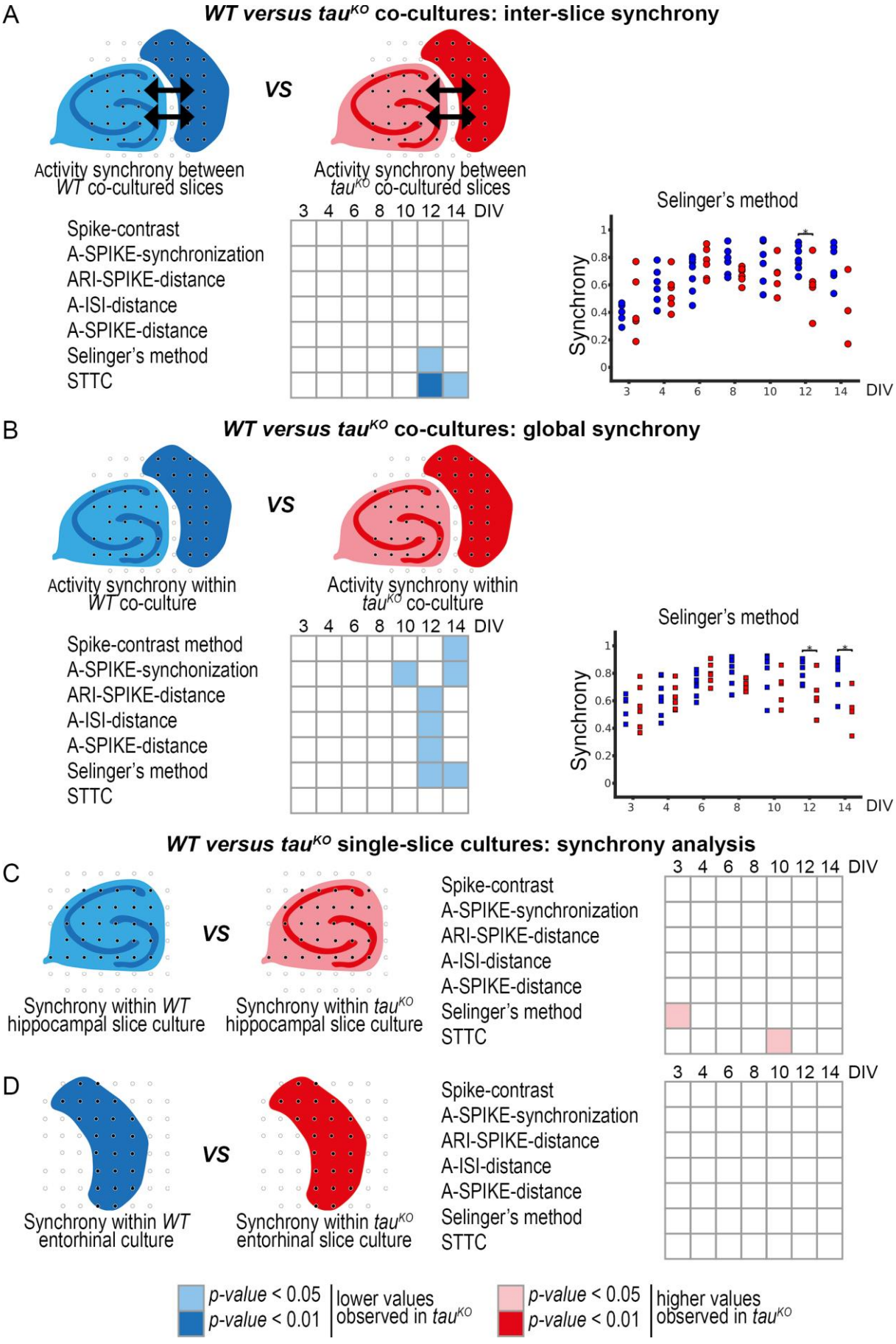
A
WT versus tauKO co-cultures: inter-slice synchrony
VS
Activity synchrony between WT co-cultured slices
Activity synchrony between tauKO co-cultured slices
3 4 6 8 10 12 14 DIV
Spike-contrast
A-SPIKE-synchronization
ARI-SPIKE-distance
A-ISI-distance
A-SPIKE-distance
Selinger's method
STTC
Selinger's method
Synchrony
DIV
B
WT versus tauKO co-cultures: global synchrony
VS
Activity synchrony within WT co-culture
Activity synchrony within tauKO co-culture
3 4 6 8 10 12 14 DIV
Spike-contrast method
A-SPIKE-synchonization
ARI-SPIKE-distance
A-ISI-distance
A-SPIKE-distance
Selinger's method
STTC
Selinger's method
Synchrony
DIV
WT versus tauKO single-slice cultures: synchrony analysis
C
VS
Synchrony within WT hippocampal slice culture
Synchrony within tauKO hippocampal slice culture
3 4 6 8 10 12 14 DIV
Spike-contrast
A-SPIKE-synchronization
ARI-SPIKE-distance
A-ISI-distance
A-SPIKE-distance
Selinger's method
STTC
D
VS
Synchrony within WT entorhinal culture
Synchrony within tauKO entorhinal slice culture
3 4 6 8 10 12 14 DIV
Spike-contrast
A-SPIKE-synchronization
ARI-SPIKE-distance
A-ISI-distance
A-SPIKE-distance
Selinger's method
STTC
p-value < 0.05
p-value < 0.01
lower values observed in tauKO
p-value < 0.05
p-value < 0.01
higher values observed in tauKO

641

Figure 4: In hippocampal-entorhinal co-cultures, tau ablation led to a reduction in the network synchrony at later stages.

(A) Comparison of the inter-slice synchrony in *WT* (blue) and *tau*^{KO} (red) co-cultures, as measured using the Spike-contrast, the A-SPIKE-synchronization, the ARI-SPIKE-distance, the A-ISI-distance, the A-SPIKE-distance, Selinger's method, and the spike time tiling coefficient (STTC) over two weeks of culture.

(B) Comparison of the global synchrony in *WT* (blue) and *tau*^{KO} (red) co-cultures, as measured using the Spike-contrast, the A-SPIKE-synchronization, the ARI-SPIKE-distance, the A-ISI-distance, the A-SPIKE-distance, Selinger's method, and the STTC over two weeks of culture.

(A, B) The graphs obtained using Selinger's method are displayed on the right.

(C) Comparison of the synchrony in *WT* (blue) and *tau*^{KO} (red) hippocampal single-slice cultures, as measured using the Spike-contrast, the A-SPIKE-synchronization, the ARI-SPIKE-distance, the A-ISI-distance, the A-SPIKE-distance, Selinger's method, and the STTC over two weeks of culture.

(D) Comparison of the synchrony in *WT* (blue) and *tau*^{KO} (red) entorhinal single-slice cultures, as measured using the Spike-contrast, the A-SPIKE-synchronization, the ARI-SPIKE-distance, the A-ISI-distance, the A-SPIKE-distance, Selinger's method, and the STTC over two weeks of culture.

The shades of blue indicate significantly lower values for the *tau*^{KO} slices and the shades of pink indicate significantly higher values for the *tau*^{KO} slices. The *p*-values are indicated by the color intensity, ranging from 0.05 to 0.01 (Wilcoxon-Mann-Whitney test).

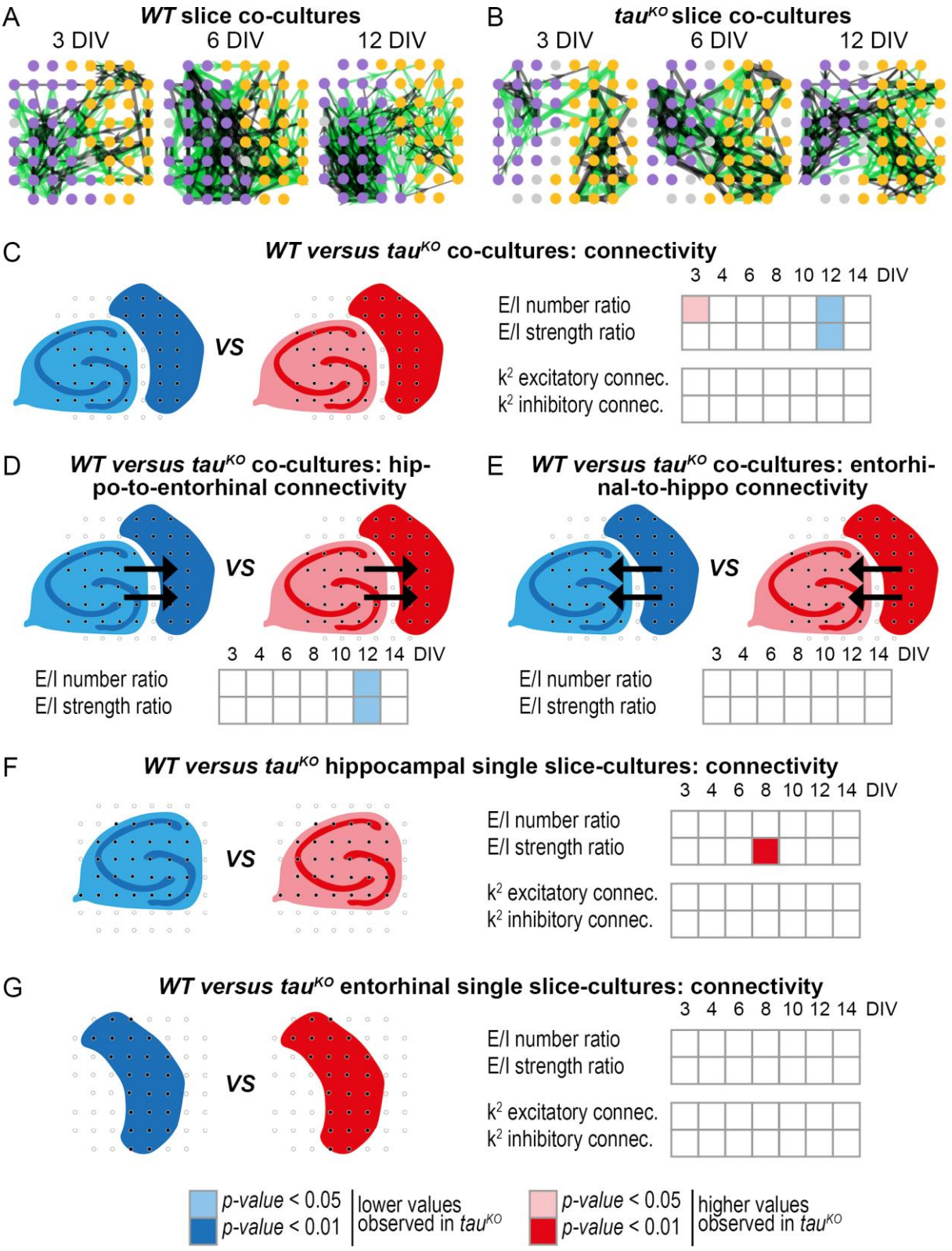

Figure 5: Analysis of the network connectivity in *WT* and *tau*^{KO} hippocampal-entorhinal co-cultures.

(A, B) Examples of network connectivity graphs for *WT* (A) and *tau*^{KO} (B) co-cultures after 3, 6, and 12 days *in vitro*. The purple and orange circles represent the electrodes in the hippocampal and entorhinal

slices, respectively. The excitatory connections are shown as green lines and the inhibitory connections as gray lines; the line thickness indicates the connection strength.

(C) Comparison of measures of connectivity in *WT* (blue) and *tau*^{KO} (red) co-cultures over two weeks: excitation/inhibition (E/I) number and strength ratios (top) and k^2 for excitatory and inhibitory connections (bottom).

(D) Comparison of measures of hippocampal-to-entorhinal connectivity in *WT* (blue) and *tau*^{KO} (red) co-cultures over two weeks: E/I number and strength ratios.

(D) Comparison of measures of entorhinal-to-hippocampal connectivity in *WT* (blue) and *tau*^{KO} (red) co-cultures over two weeks: E/I number and strength ratios.

(F) Comparison of measures of connectivity in *WT* (blue) and *tau*^{KO} (red) hippocampal single-slice cultures over two weeks: E/I number and strength ratios (top) and k^2 for excitatory and inhibitory connections (bottom).

(G) Comparison of measures of connectivity in *WT* (blue) and *tau*^{KO} (red) entorhinal single-slice cultures over two weeks: E/I number and strength ratios (top) and k^2 for excitatory and inhibitory connections (bottom).

Shades of blue indicate significantly lower values for the *tau*^{KO} slices and shades of pink indicate significantly higher values for the *tau*^{KO} slices. The color intensity indicates the *p*-values, ranging from 0.05 to 0.01 (Wilcoxon-Mann-Whitney test).

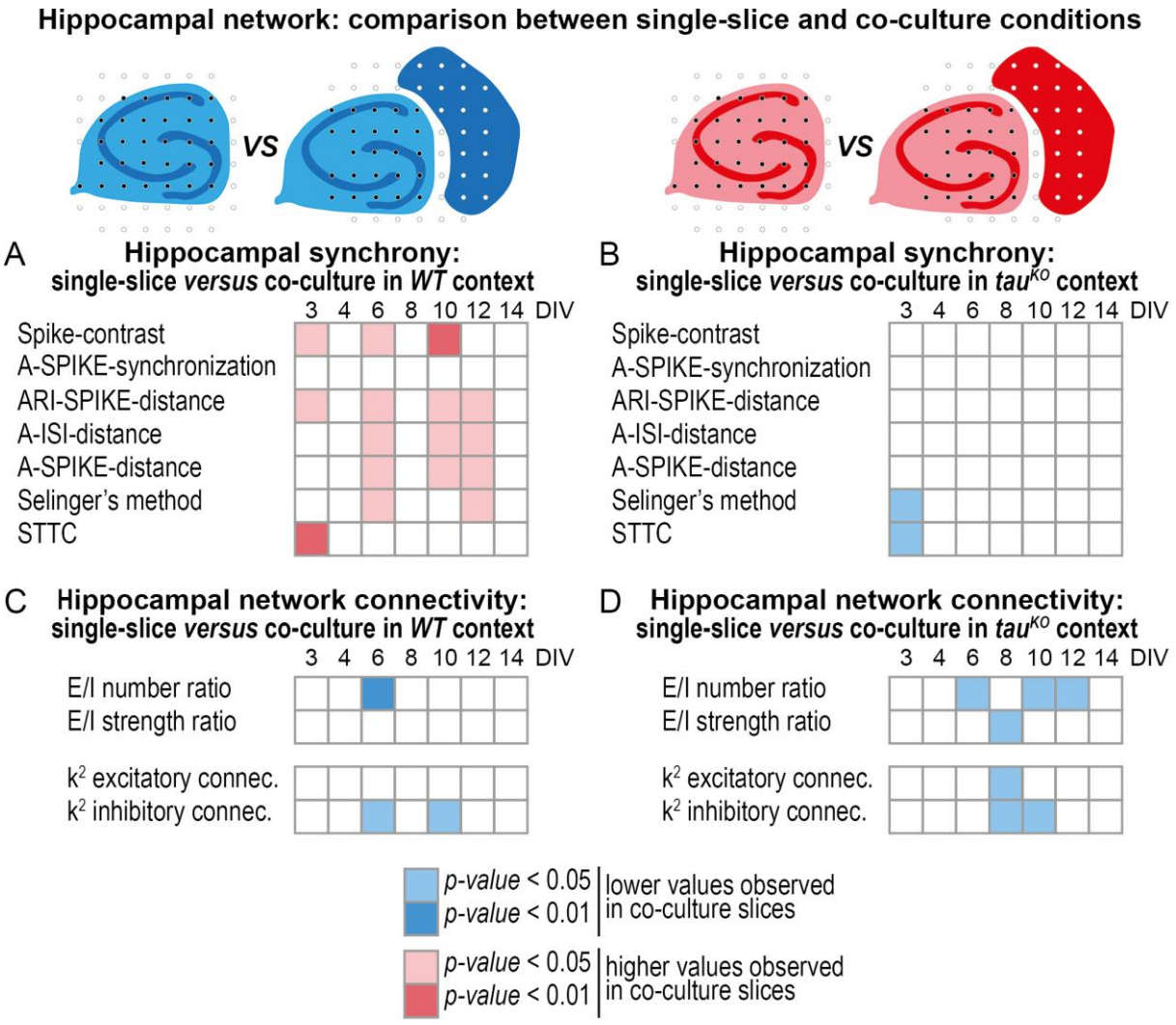

Figure 6: Tau ablation affected the evolution of the hippocampal synchrony and network connectivity within the co-cultures.

(A-B) Comparison of the hippocampal synchrony in single-slice cultures and co-cultures from wild type (A) and *tau*^{KO} (B) mice. Synchrony was measured using the Spike-contrast, the A-SPIKE-synchronization, the ARI-SPIKE-distance, the A-ISI-distance, the A-SPIKE-distance, Selinger's method, and the spike time tiling coefficient (STTC) over two weeks of culture.

(C-D) Comparison of the hippocampal within-slice connectivity in single-slice cultures and co-cultures from *WT* (C) and *tau*^{KO} (D) mice. The measures of connectivity were the excitation/inhibition (E/I) number and strength ratios (top) and the k^2 for excitatory and inhibitory connections (bottom).

Blue indicates significantly lower values for the slices in co-culture and pink indicates significantly higher values for the slices in co-culture. The color intensity indicates the *p*-values, ranging from 0.05 to 0.01 (Wilcoxon-Mann-Whitney test).

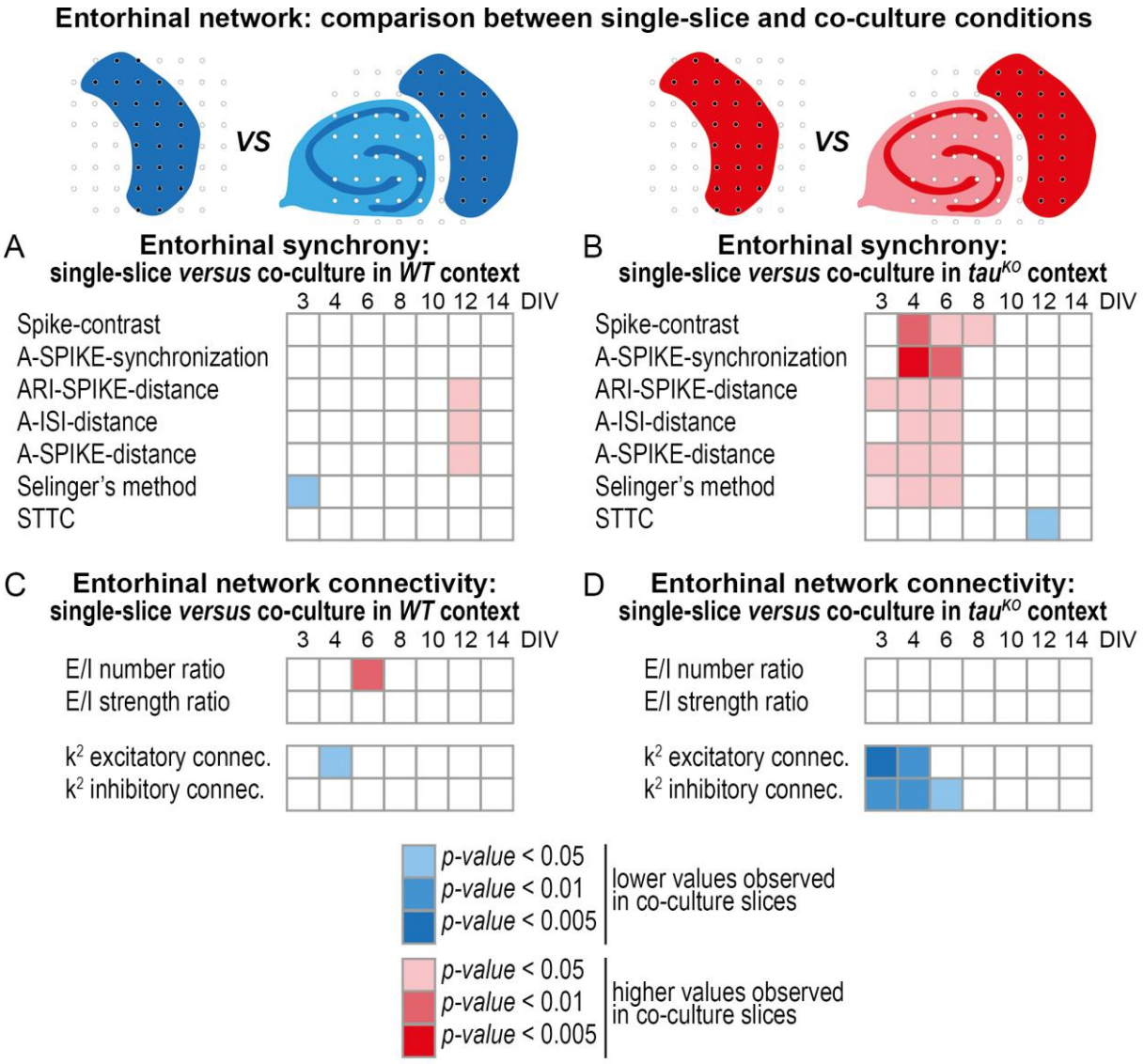

Figure 7: Tau ablation affected the evolution of the entorhinal synchrony and network connectivity within the co-cultures.

(A-B) Comparison of the entorhinal synchrony in single-slice cultures and co-cultures from wild type (A) and *tau*^{KO} (B) mice. Synchrony was measured using the Spike-contrast, the A-SPIKE-synchronization, the ARI-SPIKE-distance, the A-ISI-distance, the A-SPIKE-distance, Selinger's method, and the spike time tiling coefficient (STTC) over two weeks of culture.

706 (C-D) Comparison of the entorhinal within-slice connectivity in single-slice cultures and co-cultures
707 from *WT* (C) and *tau*^{KO} (D) mice. The measures of connectivity were the excitation/inhibition (E/I)
708 number and strength ratios (top) and the k^2 for excitatory and inhibitory connections (bottom).
709 Blue indicates significantly lower values for the slices in co-culture and pink indicates significantly
710 higher values for the slices in co-culture. The color intensity indicates the *p*-values, ranging from 0.05
711 to 0.005 (Wilcoxon-Mann-Whitney test).
712

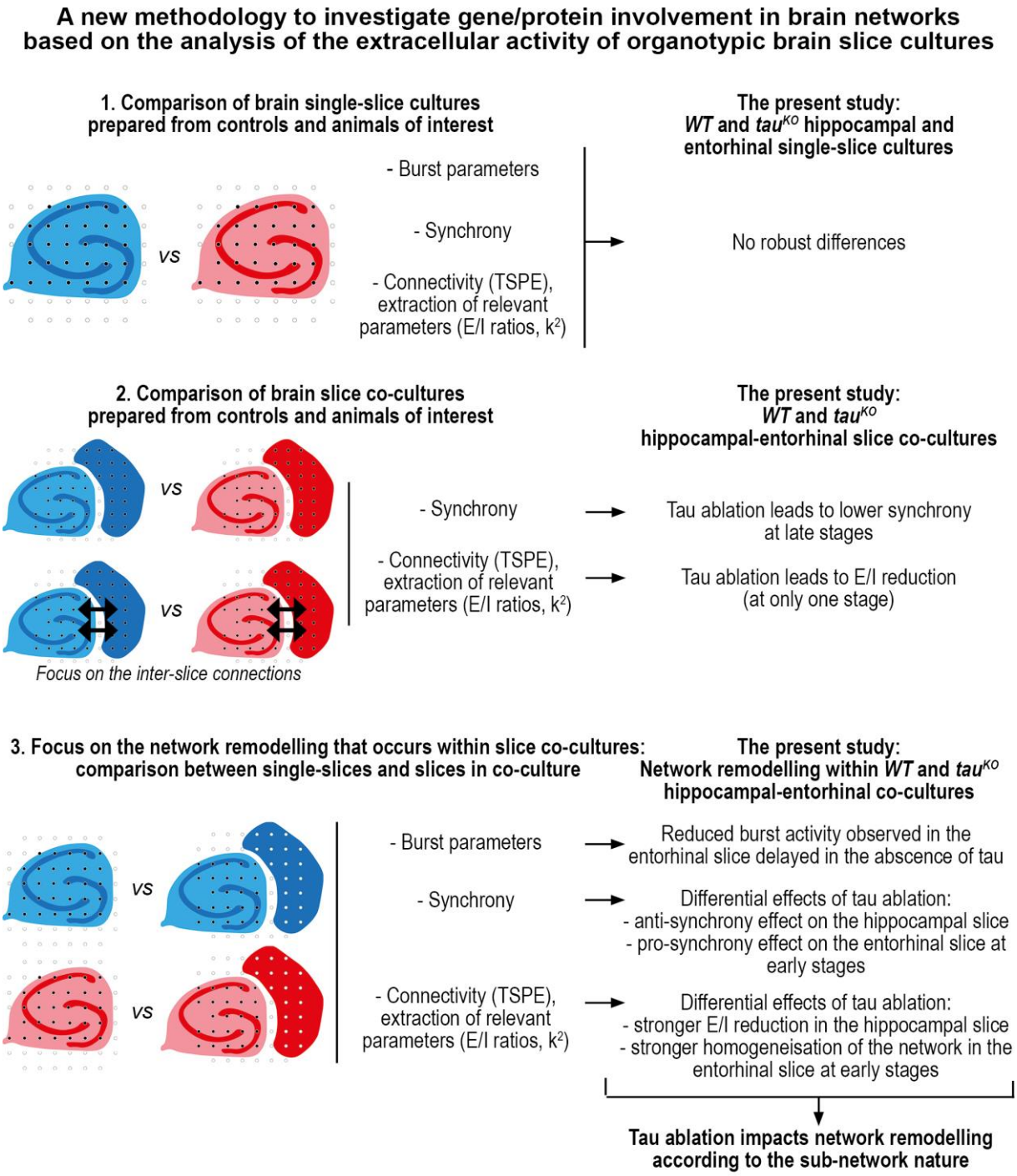

Figure 8: Diagram summarizing the methodology used for investigating the role of tau in brain-derived neural networks.

The study methodology enabled three different neural features to be analyzed: the burst activity, the synchrony, and the connectivity. The analyses were based on three main types of comparison: (1) comparison between the single-slice cultures (hippocampal or entorhinal) from control and *tau*^{KO} mice, (2) comparison between the hippocampal-entorhinal two-slice networks from control and *tau*^{KO} mice,

and (3) comparison between single-slice cultures and co-cultures from control and *tau*^{KO} mice. For each of these, the main results and conclusions are shown on the right.

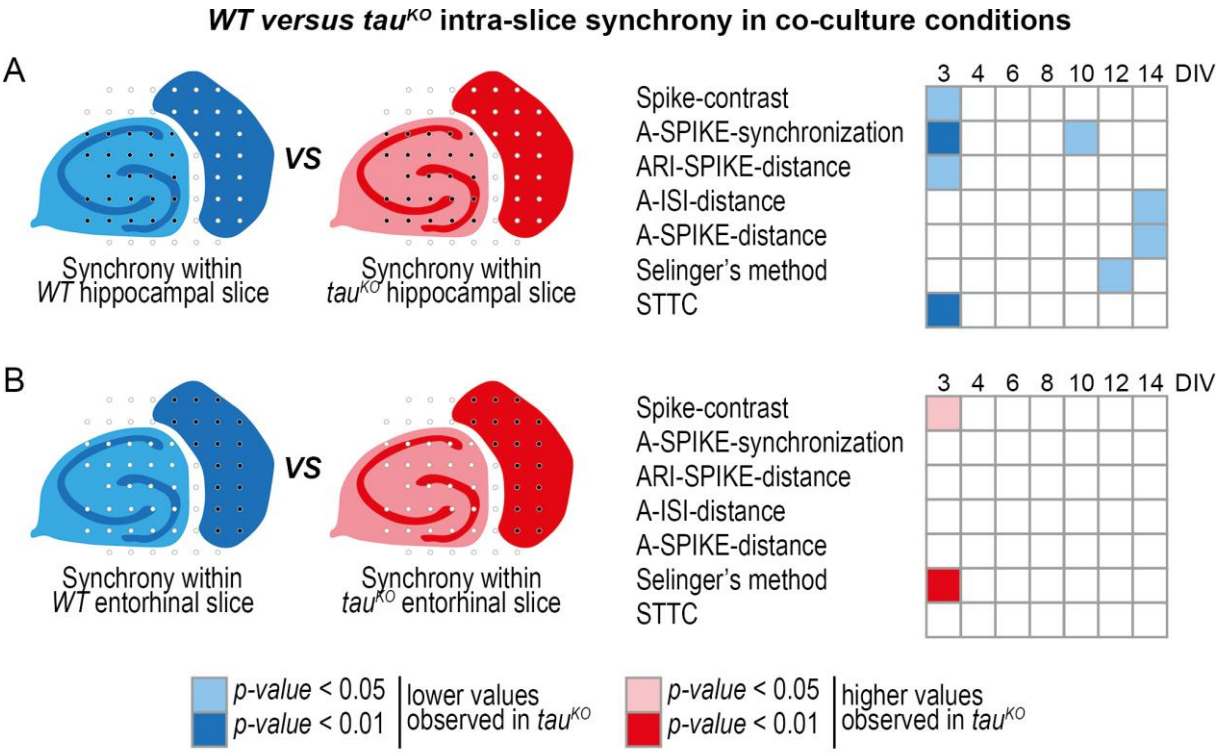

Figure 9: In hippocampal-entorhinal co-cultures, tau ablation led to a reduction in the hippocampal synchrony and an increase in the entorhinal synchrony at the beginning of the culture.

Comparison of the intra-slice synchrony in *WT* (blue) and *tau*^{KO} (red) hippocampal-entorhinal co-cultures. Synchrony was measured using the Spike-contrast, the A-SPIKE-synchronization, the ARI-SPIKE-distance, the A-ISI-distance, the A-SPIKE-distance, Selinger's method, and the spike time tiling coefficient (STTC) over two weeks of culture. The comparison between the wild type and *tau*^{KO} hippocampal slices in co-culture is shown in A. The comparison between the wild type and *tau*^{KO} entorhinal slices in co-culture is shown in B.

The shades of blue indicate significantly lower values for the *tau*^{KO} slices and the shades of pink indicate significantly higher values for the *tau*^{KO} slices. The color intensity indicates the *p*-value, ranging from 0.05 to 0.01 (Wilcoxon-Mann-Whitney test).

BIBLIOGRAPHY

Ahmed, T., Van der Jeugd, A., Blum, D., Galas, M.-C., D'Hooge, R., Buee, L., Balschun, D., 2014. Cognition and hippocampal synaptic plasticity in mice with a homozygous tau deletion. Neurobiol. Aging 35, 2474–2478. https://doi.org/10.1016/j.neurobiolaging.2014.05.005

Biundo, F., Del Prete, D., Zhang, H., Arancio, O., D'Adamio, L., 2018. A role for tau in learning, memory and synaptic plasticity. Sci. Rep. 8, 3184. https://doi.org/10.1038/s41598-018-21596-3

Boschi, A., Brofiga, M., Massobrio, P., 2021. Thresholding Functional Connectivity Matrices to Recover the Topological Properties of Large-Scale Neuronal Networks. Front. Neurosci. 15, 705103. https://doi.org/10.3389/fnins.2021.705103

Braak, H., Braak, E., 1991. Neuropathological stageing of Alzheimer-related changes. Acta Neuropathol. (Berl.) 82, 239–259. https://doi.org/10.1007/BF00308809

Braak, H., Del Tredici, K., 2016. Potential Pathways of Abnormal Tau and α-Synuclein Dissemination in Sporadic Alzheimer's and Parkinson's Diseases. Cold Spring Harb. Perspect. Biol. 8. https://doi.org/10.1101/cshperspect.a023630

Chang, C.-W., Evans, M.D., Yu, X., Yu, G.-Q., Mucke, L., 2021. Tau reduction affects excitatory and inhibitory neurons differently, reduces excitation/inhibition ratios, and counteracts network hypersynchrony. Cell Rep. 37, 109855. https://doi.org/10.1016/j.celrep.2021.109855

Chu, J.-U., Jeong, M.J., Song, K.-I., Lee, H.-C., Kim, J., Kim, Y.-J., Choi, K., Suh, J.-K.F., Youn, I., 2012. Spontaneous synchronized burst firing of subthalamic nucleus neurons in rat brain slices measured on multi-electrode arrays. Neurosci. Res. 72, 324–340. https://doi.org/10.1016/j.neures.2012.01.004

Ciba, M., Bestel, R., Nick, C., de Arruda, G.F., Peron, T., Henrique, C.C., Costa, L. da F., Rodrigues, F.A., Thielemann, C., 2020. Comparison of Different Spike Train Synchrony Measures Regarding Their Robustness to Erroneous Data From Bicuculline-Induced Epileptiform Activity. Neural Comput. 32, 887–911. https://doi.org/10.1162/neco_a_01277

Ciba, M., Isomura, T., Jimbo, Y., Bahmer, A., Thielemann, C., 2018. Spike-contrast: A novel time scale independent and multivariate measure of spike train synchrony. J. Neurosci. Methods 293, 136–143. https://doi.org/10.1016/j.jneumeth.2017.09.008

Colin, M., Dujardin, S., Schraen-Maschke, S., Meno-Tetang, G., Duyckaerts, C., Courade, J.-P., Buée, L., 2020. From the prion-like propagation hypothesis to therapeutic strategies of anti-tau immunotherapy. Acta Neuropathol. (Berl.) 139, 3–25. https://doi.org/10.1007/s00401-019-02087-9

Cutts, C.S., Eglen, S.J., 2014. Detecting pairwise correlations in spike trains: an objective comparison of methods and application to the study of retinal waves. J. Neurosci. Off. J. Soc. Neurosci. 34, 14288–14303. https://doi.org/10.1523/JNEUROSCI.2767-14.2014

De Blasi, S., Ciba, M., Bahmer, A., Thielemann, C., 2019. Total spiking probability edges: A cross-correlation based method for effective connectivity estimation of cortical spiking neurons. J. Neurosci. Methods 312, 169–181. https://doi.org/10.1016/j.jneumeth.2018.11.013

DeVos, S.L., Goncharoff, D.K., Chen, G., Kebodeaux, C.S., Yamada, K., Stewart, F.R., Schuler, D.R., Maloney, S.E., Wozniak, D.F., Rigo, F., Bennett, C.F., Cirrito, J.R., Holtzman, D.M., Miller, T.M., 2013. Antisense reduction of tau in adult mice protects against seizures. J. Neurosci. Off. J. Soc. Neurosci. 33, 12887–12897. https://doi.org/10.1523/JNEUROSCI.2107-13.2013

Dossi, E., Heine, C., Servettini, I., Gullo, F., Sygnecka, K., Franke, H., Illes, P., Wanke, E., 2013. Functional regeneration of the ex-vivo reconstructed mesocorticolimbic dopaminergic system. Cereb. Cortex N. Y. N 1991 23, 2905–2922. https://doi.org/10.1093/cercor/bhs275

Eisenman, L.N., Emnett, C.M., Mohan, J., Zorumski, C.F., Mennerick, S., 2015. Quantification of bursting and synchrony in cultured hippocampal neurons. J. Neurophysiol. 114, 1059–1071. https://doi.org/10.1152/jn.00079.2015

Fuster-Matanzo, A., Llorens-Martín, M., Jurado-Arjona, J., Avila, J., Hernández, F., 2012. Tau protein and adult hippocampal neurogenesis. Front. Neurosci. 6, 104. https://doi.org/10.3389/fnins.2012.00104

Hofmann, F., Guenther, E., Hämmerle, H., Leibrock, C., Berezin, V., Bock, E., Volkmer, H., 2004. Functional re-establishment of the perforant pathway in organotypic co-cultures on microelectrode arrays. Brain Res. 1017, 184–196. https://doi.org/10.1016/j.brainres.2004.05.044

Holth, J.K., Bomben, V.C., Reed, J.G., Inoue, T., Younkin, L., Younkin, S.G., Pautler, R.G., Botas, J., Noebels, J.L., 2013. Tau loss attenuates neuronal network hyperexcitability in mouse and Drosophila genetic models of epilepsy. J. Neurosci. Off. J. Soc. Neurosci. 33, 1651–1659. https://doi.org/10.1523/JNEUROSCI.3191-12.2013

Ittner, L.M., Ke, Y.D., Delerue, F., Bi, M., Gladbach, A., van Eersel, J., Wölfing, H., Chieng, B.C., Christie, M.J., Napier, I.A., Eckert, A., Staufenbiel, M., Hardeman, E., Götz, J., 2010. Dendritic function of tau mediates amyloid-beta toxicity in Alzheimer's disease mouse models. Cell 142, 387–397. https://doi.org/10.1016/j.cell.2010.06.036

Kent, S.A., Spires-Jones, T.L., Durrant, C.S., 2020. The physiological roles of tau and Aβ: implications for Alzheimer's disease pathology and therapeutics. Acta Neuropathol. (Berl.) 140, 417–447. https://doi.org/10.1007/s00401-020-02196-w

Khambhati, A.N., Davis, K.A., Lucas, T.H., Litt, B., Bassett, D.S., 2016. Virtual Cortical Resection Reveals Push-Pull Network Control Preceding Seizure Evolution. Neuron 91, 1170–1182. https://doi.org/10.1016/j.neuron.2016.07.039

Kimura, T., Whitcomb, D.J., Jo, J., Regan, P., Piers, T., Heo, S., Brown, C., Hashikawa, T., Murayama, M., Seok, H., Sotiropoulos, I., Kim, E., Collingridge, G.L., Takashima, A., Cho, K., 2014. Microtubule-associated protein tau is essential for long-term depression in the hippocampus. Philos. Trans. R. Soc. Lond. B. Biol. Sci. 369, 20130144. https://doi.org/10.1098/rstb.2013.0144

Lacovich, V., Espindola, S.L., Alloatti, M., Pozo Devoto, V., Cromberg, L.E., Čarná, M.E., Forte, G., Gallo, J.-M., Bruno, L., Stokin, G.B., Avale, M.E., Falzone, T.L., 2017. Tau Isoforms Imbalance Impairs the Axonal Transport of the Amyloid Precursor Protein in Human Neurons. J. Neurosci. Off. J. Soc. Neurosci. 37, 58–69. https://doi.org/10.1523/JNEUROSCI.2305-16.2016

Maestú, F., de Haan, W., Busche, M.A., DeFelipe, J., 2021. Neuronal excitation/inhibition imbalance: core element of a translational perspective on Alzheimer pathophysiology. Ageing Res. Rev. 69, 101372. https://doi.org/10.1016/j.arr.2021.101372

Nishikawa, T., Motter, A.E., Lai, Y.-C., Hoppensteadt, F.C., 2003. Heterogeneity in oscillator networks: are smaller worlds easier to synchronize? Phys. Rev. Lett. 91, 014101. https://doi.org/10.1103/PhysRevLett.91.014101

Ohara, S., Onodera, M., Simonsen, Ø.W., Yoshino, R., Hioki, H., Iijima, T., Tsutsui, K.-I., Witter, M.P., 2018. Intrinsic Projections of Layer Vb Neurons to Layers Va, III, and II in the Lateral and Medial Entorhinal Cortex of the Rat. Cell Rep. 24, 107–116. https://doi.org/10.1016/j.celrep.2018.06.014

Paglini, G., Peris, L., Mascotti, F., Quiroga, S., Caceres, A., 2000. Tau protein function in axonal formation. Neurochem. Res. 25, 37–42. https://doi.org/10.1023/a:1007531230651

Putra, M., Puttachary, S., Liu, G., Lee, G., Thippeswamy, T., 2020. Fyn-tau Ablation Modifies PTZ-Induced Seizures and Post-seizure Hallmarks of Early Epileptogenesis. Front. Cell. Neurosci. 14, 592374. https://doi.org/10.3389/fncel.2020.592374

Roberson, E.D., Halabisky, B., Yoo, J.W., Yao, J., Chin, J., Yan, F., Wu, T., Hamto, P., Devidze, N., Yu, G.-Q., Palop, J.J., Noebels, J.L., Mucke, L., 2011. Amyloid-β/Fyn-induced synaptic, network, and cognitive impairments depend on tau levels in multiple mouse models of Alzheimer's disease. J. Neurosci. Off. J. Soc. Neurosci. 31, 700–711. https://doi.org/10.1523/JNEUROSCI.4152-10.2011

Sapir, T., Frotscher, M., Levy, T., Mandelkow, E.-M., Reiner, O., 2012. Tau's role in the developing brain: implications for intellectual disability. Hum. Mol. Genet. 21, 1681–1692. https://doi.org/10.1093/hmg/ddr603

Satuvuori, E., Mulansky, M., Bozanic, N., Malvestio, I., Zeldenrust, F., Lenk, K., Kreuz, T., 2017. Measures of spike train synchrony for data with multiple time scales. J. Neurosci. Methods 287, 25–38. https://doi.org/10.1016/j.jneumeth.2017.05.028

Selinger, J.V., Pancrazio, J.J., Gross, G.W., 2004. Measuring synchronization in neuronal networks for biosensor applications. Biosens. Bioelectron. 19, 675–683. https://doi.org/10.1016/S0956-5663(03)00267-7

Sennvik, K., Boekhoorn, K., Lasrado, R., Terwel, D., Verhaeghe, S., Korr, H., Schmitz, C., Tomiyama, T., Mori, H., Krugers, H., Joels, M., Ramakers, G.J.A., Lucassen, P.J., Van Leuven, F., 2007. Tau-4R suppresses proliferation and promotes neuronal differentiation in the hippocampus of tau knockin/knockout mice. FASEB J. Off. Publ. Fed. Am. Soc. Exp. Biol. 21, 2149–2161. https://doi.org/10.1096/fj.06-7735com

Shao, E., Chang, C.-W., Li, Z., Yu, X., Ho, K., Zhang, M., Wang, X., Simms, J., Lo, I., Speckart, J., Holtzman, J., Yu, G.-Q., Roberson, E.D., Mucke, L., 2022. TAU ablation in excitatory neurons and postnatal TAU

knockdown reduce epilepsy, SUDEP, and autism behaviors in a Dravet syndrome model. Sci. Transl. Med. 14, eabm5527. https://doi.org/10.1126/scitranslmed.abm5527

Sotiropoulos, I., Galas, M.-C., Silva, J.M., Skoulakis, E., Wegmann, S., Maina, M.B., Blum, D., Sayas, C.L., Mandelkow, E.-M., Mandelkow, E., Spillantini, M.G., Sousa, N., Avila, J., Medina, M., Mudher, A., Buee, L., 2017. Atypical, non-standard functions of the microtubule associated Tau protein. Acta Neuropathol. Commun. 5, 91. https://doi.org/10.1186/s40478-017-0489-6

Tucker, K.L., Meyer, M., Barde, Y.A., 2001. Neurotrophins are required for nerve growth during development. Nat. Neurosci. 4, 29–37. https://doi.org/10.1038/82868

Vogel, J.W., Iturria-Medina, Y., Strandberg, O.T., Smith, R., Levitis, E., Evans, A.C., Hansson, O., 2020. Spread of pathological tau proteins through communicating neurons in human Alzheimer's disease. Nat. Commun. 11, 2612. https://doi.org/10.1038/s41467-020-15701-2

Vogel, J.W., Young, A.L., Oxtoby, N.P., Smith, R., Ossenkoppele, R., Strandberg, O.T., La Joie, R., Aksman, L.M., Grothe, M.J., Iturria-Medina, Y., Alzheimer's Disease Neuroimaging Initiative, Pontecorvo, M.J., Devous, M.D., Rabinovici, G.D., Alexander, D.C., Lyoo, C.H., Evans, A.C., Hansson, O., 2021. Four distinct trajectories of tau deposition identified in Alzheimer's disease. Nat. Med. 27, 871–881. https://doi.org/10.1038/s41591-021-01309-6

Witter, M.P., Doan, T.P., Jacobsen, B., Nilssen, E.S., Ohara, S., 2017. Architecture of the Entorhinal Cortex A Review of Entorhinal Anatomy in Rodents with Some Comparative Notes. Front. Syst. Neurosci. 11, 46. https://doi.org/10.3389/fnsys.2017.00046